

Cold-season atmospheric response to the natural variability of the Atlantic meridional overturning circulation

Guillaume Gastineau · Claude Frankignoul

Received: 16 February 2011 / Accepted: 23 May 2011 / Published online: 7 June 2011
© Springer-Verlag 2011

Abstract The influence of the natural variability of the Atlantic meridional overturning circulation (AMOC) on the atmosphere is studied in multi-centennial simulations of six global climate models, using Maximum Covariance Analysis (MCA). In all models, a significant but weak influence of the AMOC changes is found during the Northern Hemisphere cold-season, when the ocean leads the atmosphere by a few years. Although the oceanic pattern slightly varies, an intensification of the AMOC is followed in all models by a weak sea level pressure response that resembles a negative phase of the North Atlantic Oscillation (NAO). The signal amplitude is typically 0.5 hPa and explains about 10% of the yearly variability of the NAO in all models. The atmospheric response seems to be due primarily due to an increase of the heat loss along the North Atlantic Current and the subpolar gyre, associated with an AMOC-driven warming. Sea-ice changes appear to be less important. The stronger heating is associated to a southward shift of the lower-tropospheric baroclinicity and a decrease of the eddy activity in the North Atlantic storm track, which is consistent with the equivalent barotropic perturbation resembling the negative phase of the NAO. This study thus provides some evidence of an atmospheric signature of the AMOC in the cold-season, which may have some implications for the decadal predictability of climate in the North Atlantic region.

Keywords Atlantic meridional overturning circulation · Air-sea interactions · North Atlantic · GCM · Decadal variability

1 Introduction

The Atlantic meridional overturning circulation (AMOC) is characterized by a northward flow of warm salty surface water and a southward flow of North Atlantic Deep Water (NADW), thus transporting heat northward. The poleward oceanic and atmospheric heat transport are of similar magnitude in the tropics, but the ocean releases about 70% of its heat to the atmosphere between 20°N and 45°N (Trenberth and Caron 2001) near the western boundary current of the oceanic basins (see the review of Kwon et al. 2010), so that the atmospheric heat transport plays the dominant role at mid- to high-latitudes. Nonetheless, a strong overturning should be associated with a strong heat release from the ocean to the atmosphere, and it has been argued that it would warm Northern Europe and enhances precipitation, which is consistent with evidence from proxies of the paleo-climate. For instance, paleoproxies from the Bermuda Rise indicate a weakening of the AMOC during the Younger Dryas or the latest Heinrich cooling event (McManus et al. 2004). Although such a view is broadly supported by hosing experiments made with global climate models (see the review of Stouffer et al. 2006), the climatic impacts cannot be unambiguously attributed to the AMOC changes, as the latter were driven by strong changes in the oceanic surface layer that may also have some direct impacts.

Cause and effects may be easier to distinguish by considering the natural variability of the AMOC and its climatic signature. There is much evidence that the AMOC fluctuates even in the absence of any external forcing. However, direct observations of the AMOC remain very limited. A continuous monitoring of the AMOC across 26.5°N has begun in 2004 but the large interannual variability makes it difficult to detect low frequency changes

G. Gastineau (✉) · C. Frankignoul
LOCEAN/IPSL, Université Pierre et Marie Curie,
4 place Jussieu, BP100, 75252 Paris Cedex 05, France
e-mail: Guillaume.Gastineau@locean-ipsl.upmc.fr

(Cunningham et al. 2007). Similarly, the low-frequency variability of the deep western boundary current is masked in the observations by a strong interannual variability (Schott et al. 2006). It has been suggested that the AMOC variability can be inferred from sea surface temperature (SST) changes at decadal to multidecadal timescales (Latif et al. 2004). The multidecadal SST variability in the Atlantic Ocean shows mostly positive SST anomalies in the North Atlantic and negative anomalies in the South Atlantic (or vice versa), referred to as the Atlantic Multidecadal Oscillation (AMO) (Knight et al. 2005; Zhang 2008). The AMO has some well-established impacts on European, West-African and American climate (e.g., Rodwell et al. 1995; Sutton and Hodson 2005; Pohlmann et al. 2006; Hodson et al. 2010). However, the AMO is also influenced by global warming (Trenberth and Shea 2006) or teleconnections from the tropics (Guan and Nigam 2009), so that its climatic impact may not solely reflect an AMOC influence. Hence, despite their shortcomings, climate models may be the best tool for investigating the AMOC variability and its climatic influence.

The analysis of Atmosphere-Ocean General Circulation Model (AOGCM) simulations suggested that in many cases the stochastic forcing from the atmosphere is mainly responsible for the excitation of the decadal and multidecadal variability of the AMOC, while the time scale is controlled by oceanic processes (Mikolajewicz and Maier-Reimer 1990; Griffies and Tziperman 1995; Delworth and Greatbatch 2000; Dong and Sutton 2005). This corresponds to “one-way” interactions, where the atmospheric stochastic forcing is not significantly modified by the oceanic oscillations. However, two-way coupling between the ocean and the atmosphere was invoked by Timmermann et al. (1998) to explain the multi-decadal variability of the AMOC in their model. Strong coupled interactions were also found to play a role in the 21-year AMOC variability in the CCSM3 AOGCM (Danabasoglu 2008). Such coupled interactions were further identified and discussed in models of intermediate complexity (Eden and Greatbatch 2003; Farneti and Vallis 2009). Some other studies showed a weaker coupling between the ocean and the atmosphere, for instance Msadek and Frankignoul (2009) found in the IPSL-CM4 model a weak positive atmospheric feedback, primarily taking place in summer. Msadek et al. (2011) also suggested that the AMOC may drive a weak non-linear North Atlantic Oscillation (NAO) response during boreal winter. The presence of coupled modes of variability in models is therefore an ongoing debate and seems to depend on the model used.

The AMOC may influence the atmosphere by altering the SST and sea-ice cover, due to heat advection or shifts in the position of the main currents. There is strong observational evidence that North Atlantic midlatitude SST

anomalies have a significant influence onto the North Atlantic Oscillation (NAO) in early winter (Czaja and Frankignoul 1999, 2002). Response studies with atmospheric GCMs indicate that the winter midlatitude SST anomalies induce surface turbulent heat flux anomalies that first create a weak baroclinic perturbation in the lower troposphere, which then evolves into a stronger equivalent barotropic perturbation because of the interactions with transient eddies (Peng and Whitaker 1999; Ferreira and Frankignoul 2005; Cassou et al. 2007; Deser et al. 2007). The NAO response is also linked to Rossby wave breaking (Rivière and Orlanski 2007; Strong and Magnusdottir, 2010) and the winter eddy circulation thus acts as a non-linear positive feedback (Peng et al. 2003). Sea-ice anomalies also influence the albedo and heat exchanges at the air-sea interface, and they similarly have an impact onto the atmosphere (Magnusdottir et al. 2004; Alexander et al. 2004; Deser et al. 2007; Balmaseda et al. 2010).

It is thus timely to investigate systematically whether the changes of the AMOC have an impact on the atmospheric circulation, and to establish whether it occurs via SST or sea ice anomalies. Here, we consider control simulations with six coupled models and show that the AMOC has a significant influence on the atmosphere during the Northern Hemisphere cold-season. Section 2 is dedicated to a description of the models and simulations. In Sect. 3, we illustrate the atmospheric response to the AMOC and discuss its statistical significance. Section 4 is a discussion on the pathways of the AMOC atmospheric signature. A short discussion and conclusions are given in the last section.

2 The simulations

2.1 Models

We consider preindustrial control simulations with six coupled models used in the EC project THOR (Thermohaline Circulation at Risk?): the Bergen Climate Model (BCM, Otterå et al. 2010), HadCM3 (Vellinga and Wu 2004), IPSL-CM4 (Marti et al. 2010), IPSL-CM5 (Dufresne et al. 2010), the Kiel Climate Model (KCM, Park et al. 2009), and the Max Planck Institute for Meteorology Earth System Model (MPI-ESM, Jungclaus et al. 2010). Control simulations were chosen to better single out the influence of the AMOC variability in each model, as external forcings like volcanic aerosols or greenhouse gas changes may alter or mask the AMOC impacts. As described in Table 1, all models have low resolution. It is beyond the scope of this paper to present each model, but note that KCM and IPSL-CM5 use the same oceanic component, i.e., NEMO/OPA9, while MPI-ESM and KCM

use the same atmospheric component, i.e., ECHAM5. In addition, IPSL-CM5 is an updated version of IPSL-CM4 with a higher resolution in the atmosphere and using NEMO/OPA9 instead of NEMO/OPA8, which better parameterizes tidal mixing. Otherwise, the atmospheric, oceanic, cryospheric and land components are all different in the AOGCMs presented.

Following an initial spin-up of at least 200 years, the simulations last at least 700 years, which seems enough to characterize the significant modes of decadal and multi-decadal variability. To prevent the influence of a remaining slow model drift in some of these simulations, a quadratic least squares fit was removed from all data prior to analysis.

2.2 Interannual AMOC variability

The meridional overturning circulation in the Atlantic Ocean is diagnosed with the meridional streamfunction. Figure 1 shows the mean AMOC of each AOGCM, a positive streamfunction indicating a clockwise rotation. The major feature is the positive overturning circulation cell between the surface and about 2500 m depth, reflecting the northward transport of surface water, its sinking mostly near 60°N, and the southward return flow of NADW. At larger depth, there is a weaker negative circulation cell due to the northward penetration of Antarctic Bottom Water. For all models, the maximum overturning is found around 30°N. Estimations from observations suggest a maximum overturning circulation of about 15 Sv (Ganachaud and Wunsch 2000), therefore IPSL-CM4, IPSL-CM5, and to a lesser extent, KCM underestimate the AMOC.

The first Empirical Orthogonal Function (EOF) of the yearly AMOC between 30°S and 80°N is presented in Fig. 2. To calculate the EOFs, the Atlantic meridional streamfunction was weighted by the squared root of the ocean layer thickness to give equal weight to each area, which emphasizes the deeper ocean variability. Here,

EOFs are displayed as regression maps onto the corresponding normalized Principal Component (PC), so that the EOFs show the typical amplitude of the fluctuations. For all models but MPI-ESM, the main mode of yearly variability is a large positive cell occupying the whole ocean depth as in most oceanic (Eden and Willebrand 2001; Deshayes and Frankignoul 2008; Bentsen et al. 2004) and coupled (Vellinga and Wu 2004; Msadek and Frankignoul 2009) models, which presumably reflects the dominant role of the western boundary in transmitting signals originating in the subpolar North Atlantic, either by wave propagation or by density advection along the deep western boundary current. The typical amplitude of the AMOC variability ranges between 0.6 and 1.4 Sv. The maximum is centered either in the tropical North Atlantic in BCM and IPSL-CM4 or near 45°N in HadCM3 and IPSL-CM5, depending of the main mechanism responsible for the yearly AMOC variability in models. These EOFs differ from the one of the low-frequency AMOC variability, classically obtained with a 10-year low pass filter which have a maximum further north between 30°N and 60°N (Vellinga and Wu 2004; Msadek and Frankignoul 2009).

In KCM, the cell is centered in the tropical South Atlantic, which reflects an important multi-centennial variability driven by the Southern Ocean (Park and Latif 2008). In MPI-ESM, the first EOF is similar to the others only when the AMOC is considered between 0°N and 80°N, as done in the rest of this paper. Indeed, when using the whole Atlantic domain from 30°S to 80°N, the first EOF in MPI-ESM has a very different pattern with a strong dipolar cell in the Southern Hemisphere, negative between 0 and 2,000 m and positive below (or vice versa), with a typical intensity of 2 Sv (not shown), and a clear link to ENSO (El Niño Southern Oscillation). The frequency spectrum of the first PC of the AMOC (not shown) is mostly red in each model, with significant interannual to multi-decadal variability, as in other state-of-the-art coupled models (Danabasoglu 2008;

Table 1 Presentation of the models

Model name	Horizontal grid (Atm)	Horizontal grid (Ocn)	Vertical levels (Atm) (hybrid)	Vertical levels (Ocn)	Duration (year)
BCM	128 × 64 Spectral	260 × 240 Conformal	31	35 (isopyc.)	700
HadCM3	96 × 73 Regular	278 × 139 Lat/long	19	20 (z)	700
IPSL-CM4	96 × 71 Regular	181 × 149 Conformal/bipolar	19	31 (z)	1,000
IPSL-CM5	96 × 96 Regular	181 × 149 Conformal/bipolar	39	31 (z)	1,000
KCM	96 × 48 Spectral	181 × 149 Conformal/bipolar	19	31 (z)	1,000
MPI-ESM	96 × 48 Spectral	101 × 122 Conformal/bipolar	19	40 (z)	1,000

The resolution and grid properties are illustrated

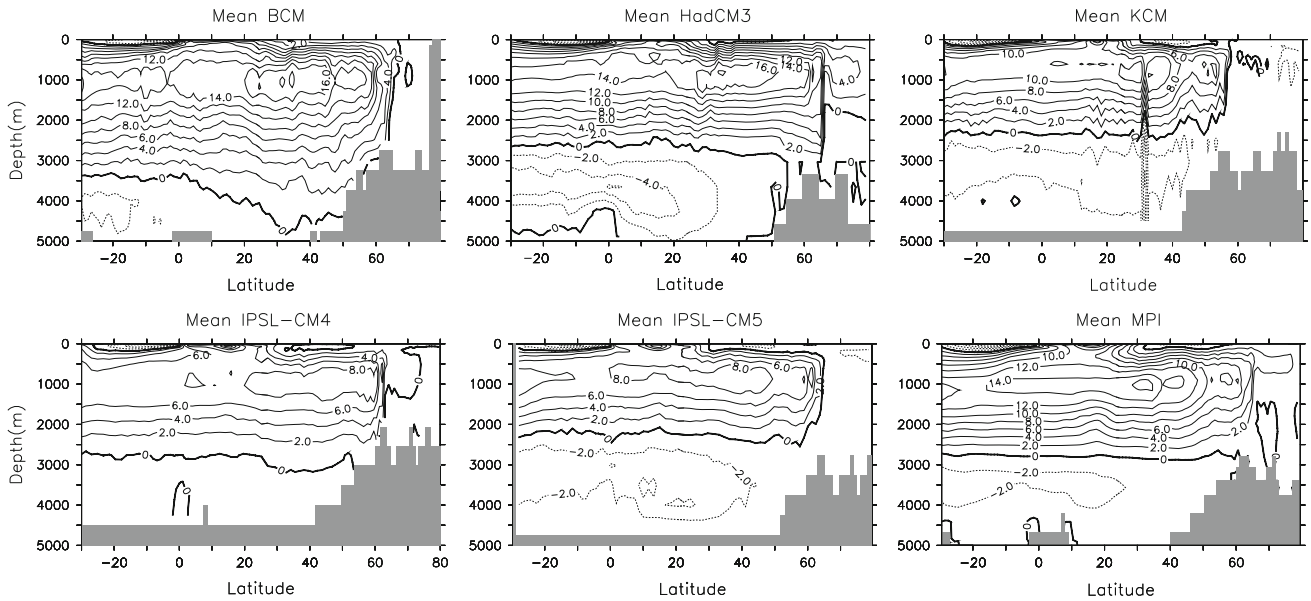


Fig. 1 Mean overturning streamfunction in the Atlantic Ocean, in Sv

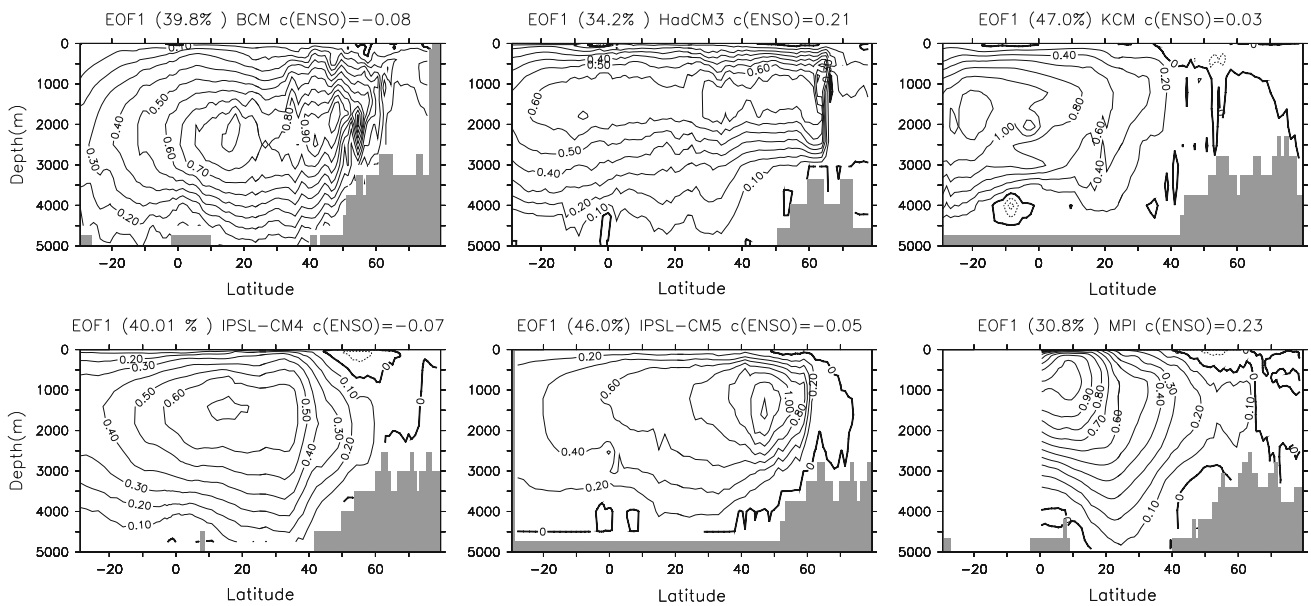


Fig. 2 EOF1 of the meridional overturning streamfunction, in Sv. The variance fraction of EOF1 and the in phase correlation of the first PC with an index of ENSO, $c(\text{ENSO})$, are given at the top of each panel. The EOF time series were normalized so that the figure

indicates typical magnitudes. For MPI-ESM, the meridional streamfunction is used only in the 0° – 80° N region, to remove the influence of tropical variability

Frankcombe et al. 2010). IPSL-CM5 is the only model that shows a significant spectral peak, which corresponds to a 20-year periodicity.

In HadCM3, there is a significant correlation between the first PC of the yearly AMOC and an ENSO index (Vellinga and Wu 2004). To see whether this is the case in the other models, we have defined an ENSO index as the first PC of the equatorial Pacific SST, defined over 12° N– 12° S,

80° W– 100° E. The correlation between the first PC of the AMOC and the ENSO index is always strongest without time lag and is given in Fig. 2. The correlation is large and significant in MPI-ESM and HadCM3 (0.23 and 0.21 respectively), while it is very weak in the other models. Since ENSO teleconnections may mask the AMOC influence onto the atmospheric circulation, the ENSO signal will be removed as discussed below.

3 Atmospheric response to the AMOC

3.1 Method

To estimate the atmospheric response to the AMOC, we use the sea level pressure (SLP) in the North Atlantic sector (10°N–80°N, 100°W–40°E) and ψ , the Atlantic meridional overturning streamfunction. Yearly averages are used for ψ to highlight the low frequencies, while three-month seasonal means are used for the atmosphere to represent its seasonality. The atmospheric signal in the North Atlantic sector may also be influenced by co-varying SSTs at other locations. As ENSO significantly affects the Atlantic SLP through atmospheric teleconnections (Mathieu et al. 2004; Timmermann et al. 2007), much of the ENSO influence was removed by replacing the anomalies of the meridional overturning streamfunction and SLP, $X(t)$ and $\psi(t)$, by $X(t) - aN_1(t) - bN_2(t)$ and $\psi(t) - cN_1(t) - dN_2(t)$, where $N_1(t)$ and $N_2(t)$ are the first two PCs of the SST over the equatorial Pacific Ocean (12.5°S–12.5°N, 100°E–80°W), and a , b , c and d are regression coefficients determined by least squares fit for each grid point, using yearly averaged values for $\psi(t)$ and three-month seasonal means for $X(t)$. Note that non-linear effects are neglected, so that the ENSO signal may not be completely removed.

Lagged Maximum Covariance Analysis (hereafter MCA) has been widely used to highlight the influence of the ocean on the atmosphere (Czaja and Frankignoul 1999, 2002; Frankignoul and Kestenare 2005). As the time scale of the ocean and atmosphere are well separated, when the ocean leads by more than the atmospheric persistence, the relationships between oceanic and atmospheric fields are indicative of the influence of the ocean on the atmosphere. The ocean influence is masked in phase or when the ocean follows, due to the larger impact of the atmosphere on the ocean. The MCA isolates pair of spatial patterns and their associated time series by performing a singular value decomposition of the covariance matrix between two fields (Bretherton et al. 1992). Here, the two dimensional fields of SLP, $\mathbf{X}(t)$ (latitude-longitude), at time t and Atlantic meridional overturning streamfunction, $\psi(t - \tau)$ (latitude-depth), at time $t - \tau$ are expanded into K orthogonal spatial patterns:

$$\mathbf{X}(t) = \sum_{k=1}^K \mathbf{u}_k a_k(t) \quad (1)$$

$$\psi(t - \tau) = \sum_{i=1}^K \mathbf{v}_i b_i(t - \tau) \quad (2)$$

where τ is the time lag. \mathbf{u}_k and \mathbf{v}_k are the left and right singular vectors, which give the full spatial structure of the main mode of covariance between the AMOC and the SLP, with $\mathbf{u}_k \cdot \mathbf{u}_l = \delta_{kl}$, $\mathbf{v}_i \cdot \mathbf{v}_j = \delta_{ij}$. The covariance between a_k

and b_k , the times series associated with the left and right singular vectors, respectively, is maximum for $k = 1, 2, \dots$ and the time series are orthogonal to one another between the two fields, $\text{cov}(a_k, b_i) = \sigma_k \delta_{ki}$. Here, σ_k is the covariance explained by the pair of left and right singular vectors, \mathbf{u}_k and \mathbf{v}_k . In the MCA, the SLP is weighted by the square root of the cosine of the latitude, and ψ is weighted by the square root of the oceanic layer thickness to give equal weight to each area.

The homogeneous maps for the ocean and heterogeneous maps for the atmosphere, defined as the projections of $\psi(t - \tau)$ and $\mathbf{X}(t)$ onto $b_k(t - \tau)$, may be shown to study the influence of the ocean onto the atmosphere, when the ocean leads. When studying the oceanic response to the atmosphere, it is preferable to show the heterogeneous AMOC and the homogeneous SLP, which are the projections of $\psi(t - \tau)$ and $\mathbf{X}(t)$ onto $a_k(t)$. In both cases, linear relations between variables are preserved (Czaja and Frankignoul 2002).

The relationships are usually weak in extratropical air-sea interaction studies when the ocean leads the atmosphere, so that careful statistical testing is required to identify whether the modes of variability are meaningful. For each lag, the statistical significance of the squared covariance and correlation between the time series $a_k(t)$ and $b_k(t - \tau)$ is assessed with a Monte Carlo approach, by comparing the squared covariance and correlation to that of a randomly scrambled ensemble. We randomly permute the SLP time series by blocks of 3 years to reduce the influence of serial autocorrelation, and perform an MCA. We repeat this analysis 100 times. The estimated significance level is the percentage of randomized squared covariance (correlation) that exceeds the squared covariance (correlation) being tested. It is an estimate of the risk of rejecting the null hypothesis (there is no relation between the SLP and the AMOC), and a smaller significance level indicates the presence of stronger evidence against the null hypothesis.

3.2 Influence of the seasonal cycle

The MCA was calculated by using seasonal averages for SLP in JFM (January-February-March), AMJ (April-May-June), JAS (July-August-September) and OND (October-November-December). The seasons are chosen in order to include the early spring (March) in winter, as the oceanic mixed layer is deeper and the SST more persistent during this period, which may enhance the impacts of the ocean onto the atmosphere. In KCM and MPI-ESM, the atmospheric response to the AMOC would not have been seen if DJF (December-January-February) was used for winter. The covariance of the first MCA mode is shown in Fig. 3 as a function of lag. In all models, the covariance between

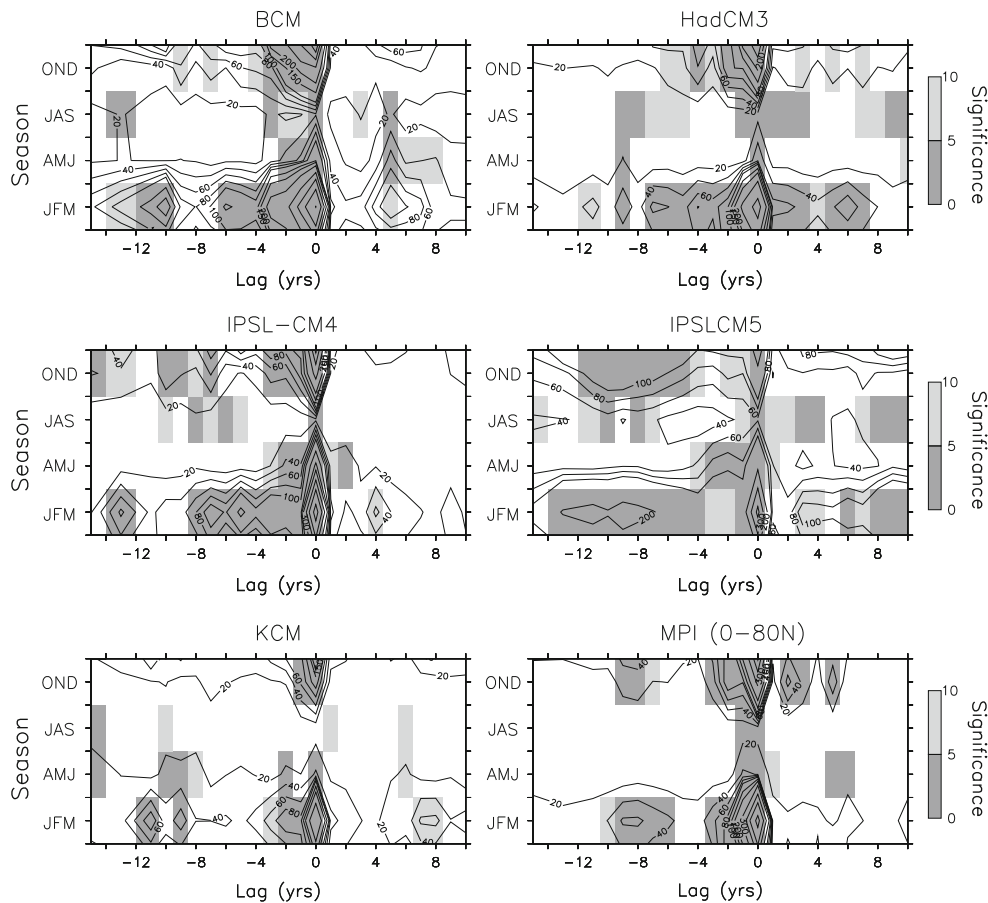


Fig. 3 Covariance of the first MCA mode between SLP and AMOC (contour), in hPa Sv. The *gray shades* indicate the squared covariance significance level, in %. The lag is positive (negative) when the AMOC (SLP) leads

the AMOC and the northern Atlantic SLP is strongest during winter, when SLP and AMOC are in phase, or when SLP leads (lag < 0), reflecting the atmospheric forcing of the AMOC, which is strongest and most efficient during the cold season, from November to April. When the AMOC leads (lag > 0), the covariance is much weaker and less significant, but it is still largest and most significant in winter (JFM), except for MPI-ESM, where it is maximum in fall (OND). We also note that there are significant covariances when the AMOC leads SLP in spring (AMJ) or summer (JAS), depending on the model.

In the following, we only focus on the cold season that corresponds to JFM or OND, where midlatitudes SST and sea-ice anomalies have been shown to have a significant influence onto the atmosphere (Czaja and Frankignoul 2002; Deser et al. 2007). For each model, we select the season yielding the most significant atmospheric response.

3.3 Response of the AMOC to the atmospheric forcing

Figure 4 shows the covariance and correlation of the first MCA mode between the cold-season (OND or JFM) SLP

and the yearly AMOC as a function of time lag. For all models, the large covariance at lag 0 reflects the fast response of the AMOC to stochastic NAO forcing. The covariance tends to be larger when the SLP is taken in winter, as the atmospheric internal variability is stronger in winter than in fall. As illustrated in Fig. 5, the winter SLP pattern of the first MCA mode represents the NAO, displayed here in a positive phase (positive pressure anomaly over the Azores and negative pressure over Iceland). The NAO patterns are similar to the observed ones (Hurrell et al. 2003). Most models show a largely barotropic negative AMOC anomaly in the subpolar regions and a positive one in the subtropics, consistent with the anomalous Ekman pumping and the deep return flow driven by the NAO surface wind stress. Such a fast response has been discussed by Eden and Willebrand (2001), Deshayes and Frankignoul (2008), and others.

The covariance between the AMOC and the SLP is weaker when the atmosphere leads the ocean by a few years (see Figs. 3, 4). IPSL-CM5 shows a stronger impact when the atmosphere leads the AMOC by 9 to 11 year, which is associated to the 20-year cycle of the AMOC in

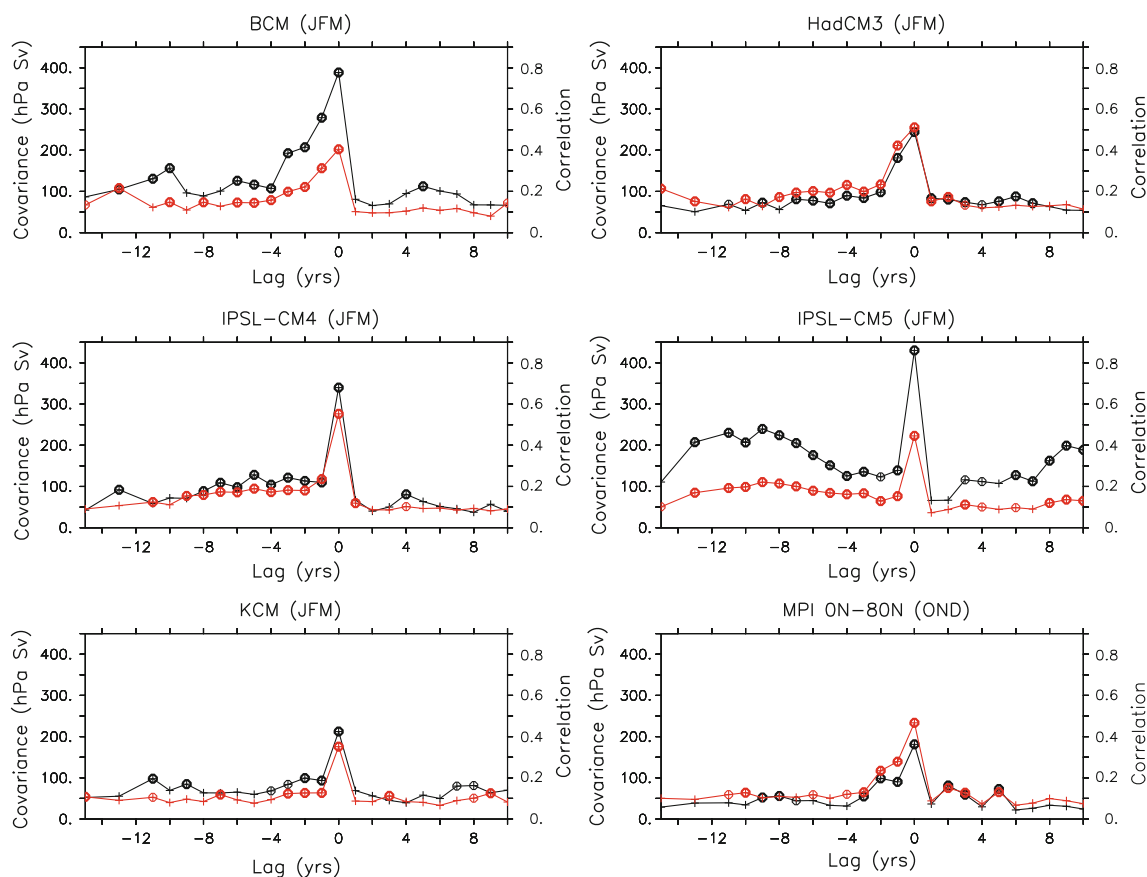


Fig. 4 Covariance and correlation of the first MCA mode between the cold-season SLP and the yearly AMOC. The covariances (correlations) are shown with black (red) lines. The thick (thin) circles show the lags where the significance level is lower than 5% (10%)

this model. The response of the AMOC when the atmosphere leads the ocean by 3 years is illustrated in Fig. 6. In all models but IPSL-CM4 and IPSL-CM5, a positive phase of the NAO is followed 3 years later by an AMOC intensification, mostly in the Northern Hemisphere. Such a delayed response is common in ocean models and it largely reflects the delayed baroclinic response of the AMOC to the heat flux anomalies induced by the NAO (Eden and Willebrand 2001). For IPSL-CM4 and IPSL-CM5, the AMOC shows a positive AMOC anomaly in the subpolar regions, but a negative one south of 40°N . Msadek and Frankignoul (2009) previously found that the East Atlantic Pattern (EAP), the second EOF of the SLP, is more important in driving the low-frequency variability of the AMOC in IPSL-CM4, which would be seen in the second MCA mode. This is also the case of IPSL-CM5. These singularities may reflect the unrealistic location of the subpolar deep convection zones in these models.

The response of the AMOC to the atmospheric forcing was also briefly investigated when the atmosphere leads the AMOC by a larger lags (not shown). The results were mostly similar to the ones in Fig. 6, except for IPSL-CM4

and IPSL-CM5 where role of the EAP is stronger. As our emphasis is on the AMOC influence on the atmosphere, the AMOC response to the atmosphere is not discussed further.

3.4 Atmospheric response to the AMOC

When the AMOC leads the atmosphere, the covariance of the first MCA mode is significant, albeit in a limited fashion, at one or several lags between 1 and 10 year, depending on the model (see Fig. 4). For HadCM3 and IPSL-CM5, the covariance is significant for several lags from 1 to 7 year and from 3 to 10 year, respectively, while for the other models the covariance is only significant at one or two specific lags during the cold season. At a short lag of 1 or 2 year, the first MCA mode is often less significant and the covariance is weaker than at larger lag, as the oceanic circulation may take longer to affect critically the surface boundary conditions for the atmosphere. At lag larger than 10 year, the covariance and correlation are smaller and less significant, even if they remain significant at the 5% level for a few additional lags in IPSL-CM5, due to the 20-year cycle of the AMOC in this model.

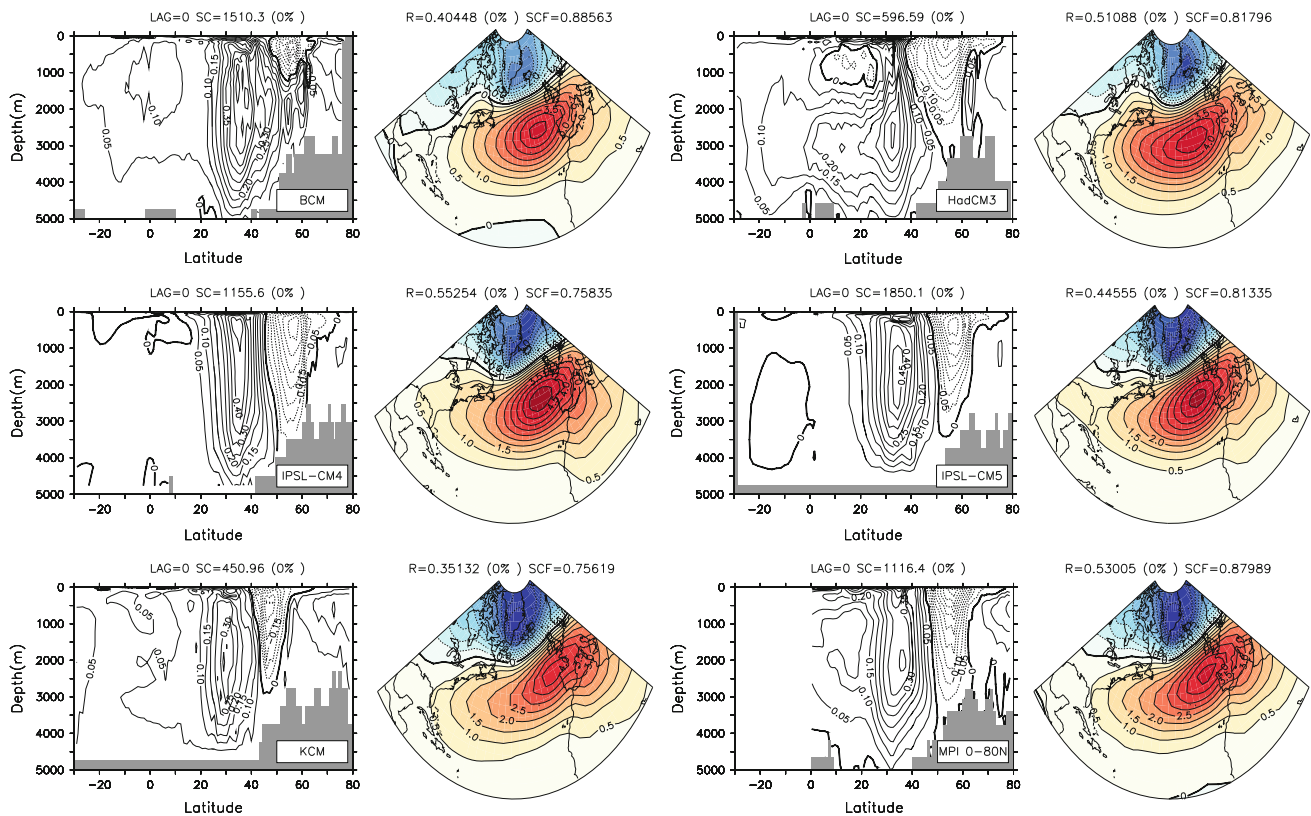


Fig. 5 Homogeneous map of the JFM SLP (hPa) and heterogeneous map of the yearly AMOC (Sv) for the first MCA mode, when the atmosphere and the AMOC are in phase (lag 0). SC is the squared covariance, in $10^2 \text{ hPa}^2 \text{ Sv}^2$. R is the correlation. SCF is the SC

fraction of the MCA first mode. Estimated statistical significance levels are indicated in % for SC and R. The MCA time series were normalized so that the typical magnitudes are given

The homogeneous AMOC and heterogeneous SLP maps of the first MCA mode are given in Fig. 7, the lag corresponding to the most significant signal in each model. The AOGCMs show a consistent response, a NAO-like SLP pattern following by 4–9 year an intensified AMOC. The AMOC pattern is generally similar to the first EOF of the AMOC (see Fig. 2), while the atmospheric pattern broadly corresponds to a negative phase of the NAO. The spatial correlation between the SLP heterogeneous maps in Fig. 7 and the NAO pattern in each model ranges between -0.81 and -0.97 . However, in many cases (IPSL-CM4, KCM and BCM), the zero-line between the positive and negative SLP anomalies is located further southward than in the NAO, so that it also resembles a northward-shifted EAP. At the other positive lags where the first MCA mode is significant, the atmospheric and oceanic patterns are similar to those shown in Fig. 7. An exception occurs at lag 3 for MPI-ESM, where the AMOC is only intensified north of 35°N , but reduced south of 35°N . This suggests that the subpolar region is key to the AMOC influence on the NAO in this model.

The amplitude of the winter SLP response typically ranges between 0.4 and 0.8 hPa, depending on lag and

model, while the AMOC amplitude is typically about 1 Sv, comparable to that of the first EOF of the AMOC. Hence, the atmospheric response is weak, roughly ten time smaller than the interannual SLP fluctuations. Correspondingly, the correlation between the time series associated to the left and right singular vectors only ranges between 0.10 and 0.18, so the AMOC could only explain a small fraction of the cold-season NAO fluctuations. However, as the AMOC spectrum is red but the NAO one is white, and the relative AMOC impacts onto the SLP fluctuations would be more important at low frequency, as discussed in Sect. 5.

In order to verify the statistical significance of the atmospheric response to the AMOC, we have regressed the cold-season ENSO-removed SLP onto the normalized time series associated with the AMOC right singular vector of the first MCA mode, $b_1(t - \tau)$, hereafter denoted by MOC_y , with a lag corresponding to the most significant MCA mode, separately for the two halves of each simulation (Fig. 8). The significance level is estimated at each grid points by Monte Carlo analysis using random permutations of the SLP anomalies by blocks of 3 years. Although the signal-to-noise ratio is low, for each model a significant broad NAO-like dipole emerges for both halves,

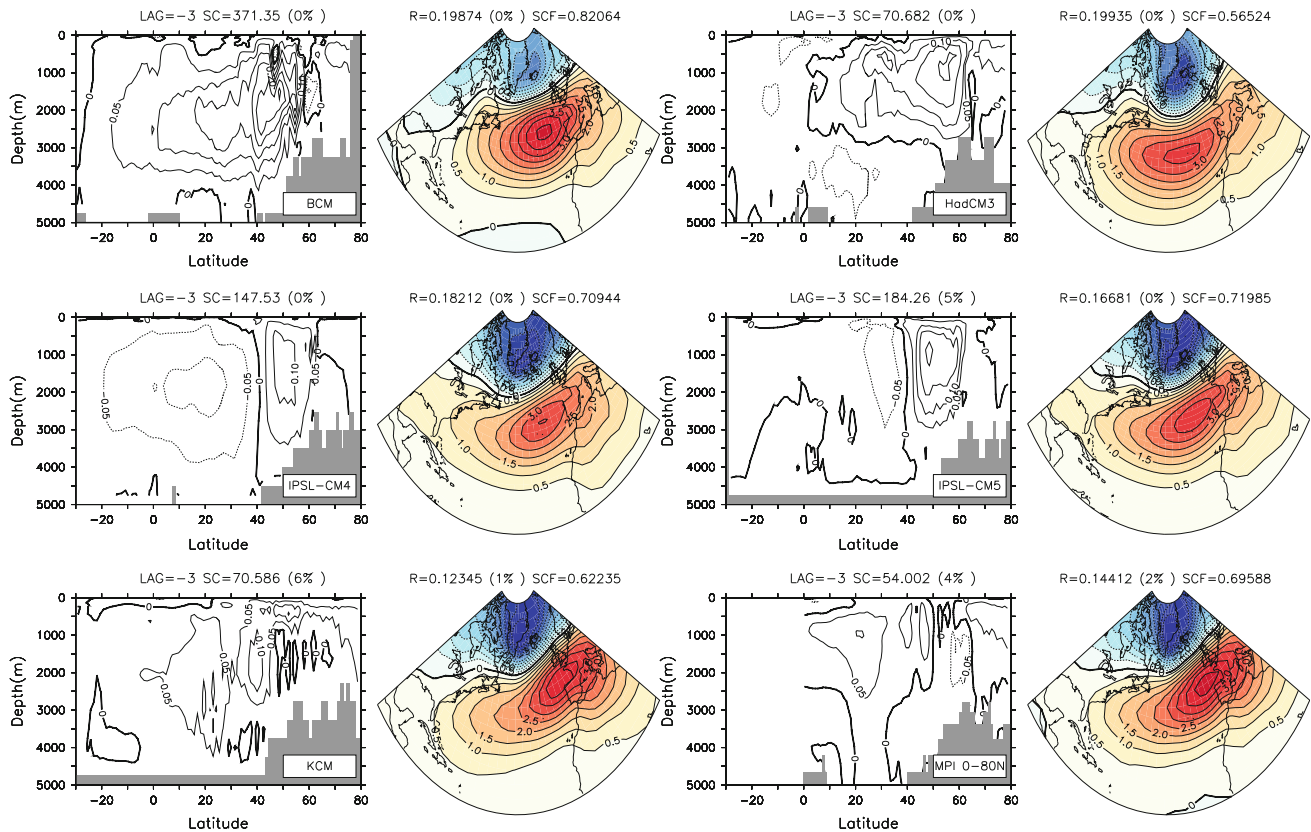


Fig. 6 Same as Fig. 6, but for when the JFM SLP leads the AMOC by 3 years (lag -3)

with the same polarity. Hence, the AMOC influence onto SLP found in the MCA analysis appears to be robust.

The vertical extent of the atmospheric changes is also investigated. The response of the ENSO-removed geopotential height at the 850-, 500- and 200-hPa levels is presented in Fig. 9 with regressions onto MOCy for IPSL-CM4. The atmospheric response is equivalent barotropic. Indeed, the polarity and location of the dipolar anomalies of the geopotential height are similar to those of the SLP (see Fig. 7). The changes of the 200-hPa and 500-hPa geopotential heights are also studied in the other models, and similarly reveal an equivalent barotropic response. This is consistent with the response to midlatitude SST anomalies found in atmospheric response studies (e.g., Lau and Nath 1990; Peng and Whitaker 1999; Deser et al. 2007).

4 Climate impact of the AMOC

4.1 Links with SST and sea-ice cover

The patterns of SST and sea-ice cover associated with the AMOC changes help to understand the mechanisms

leading to the atmospheric response. Figures 10 and 11 show the regressions of the SST and sea-ice cover, respectively, onto MOCy. The color scale is non-linear, to display the weak anomalies. As before, the significance level was established by Monte Carlo analysis, with permutations of SST or sea-ice cover by blocks of 3 years. For consistency, the ENSO variability was also removed from the SST and sea-ice anomalies.

As shown in Fig. 10 (right panels), the SST anomalies that correspond to the atmospheric response are strongest in the North Atlantic region, suggesting that the atmospheric response to the AMOC is largely controlled by air-sea interactions in the North Atlantic region. In KCM, strong SST anomalies are also found in the Southern Hemisphere midlatitudes and subtropics, reflecting the strong link between the AMOC and the Southern Ocean (Park and Latif 2008). For the other models, the SST anomalies are always lower than 0.05 K and hardly significant in the tropics. In BCM, HadCM3, IPSL-CM4 and IPSL-CM5, small negative SST anomalies are seen in the Southern Ocean. This is consistent with the AMOC-driven increased oceanic northward heat transport in the Atlantic ocean. In some case, the anomalies are also found in the Indian and Pacific sector of the Southern Ocean. In

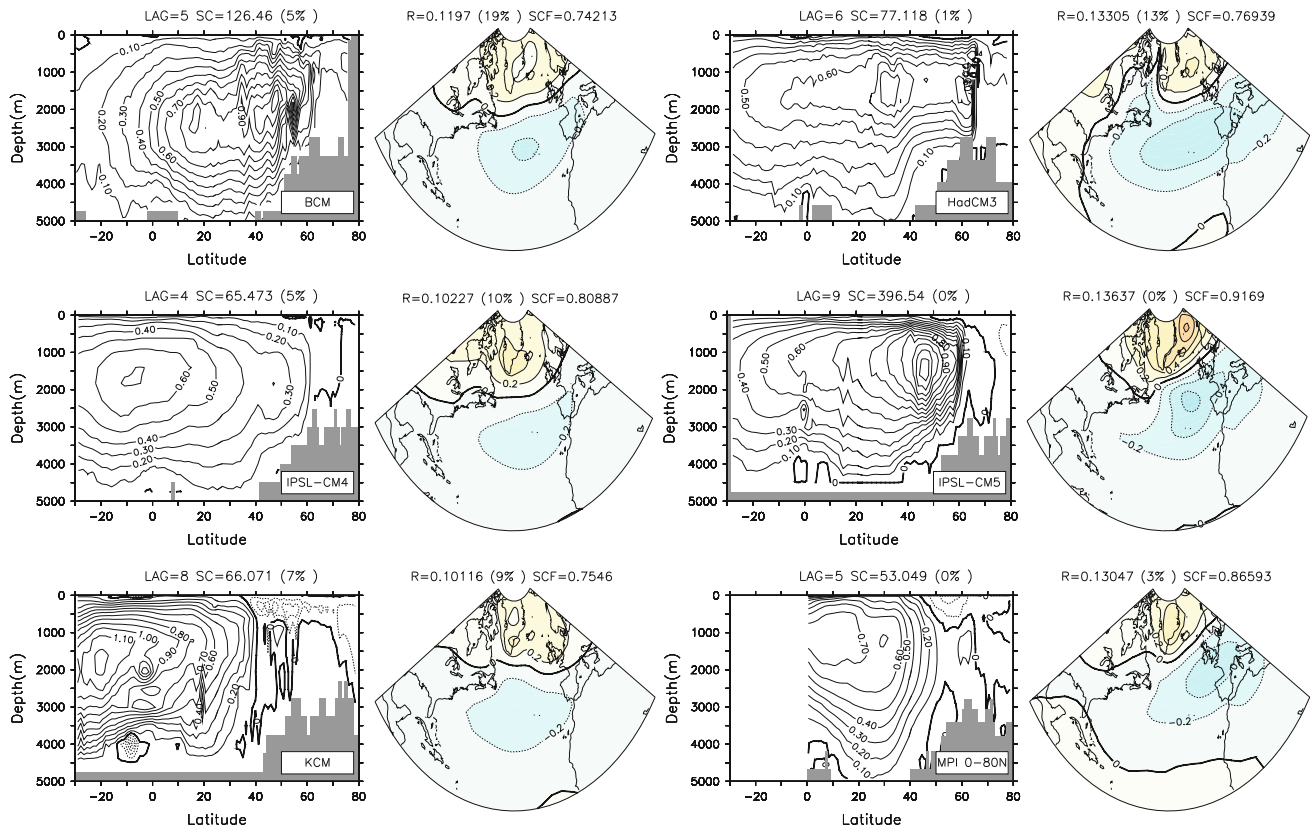


Fig. 7 Same as Fig. 5, but for the homogeneous map of AMOC (Sv) and heterogeneous map of cold-season SLP (hPa) for the most significant delayed atmospheric response to the AMOC. The lag, in

year is indicated for each model. The cold-season SLP corresponds to JFM, except for MPI-ESM, where it corresponds to OND

HadCM3, IPSL-CM4 and IPSL-CM5, small SST anomalies (< 0.1 K) are also found in the North Pacific.

An enlarged view of the SST anomalies in the North Atlantic is presented in Fig. 10 (center panels). In each model there are extended positive SST anomalies located in the subpolar gyre region, between 45°N and 65°N , when the atmospheric response to the AMOC is the strongest. The models HadCM3 and IPSL-CM5 show the largest positive SST anomalies in the subtropical region, which corresponds to a more significant atmospheric response in these two models. In parallel, there is a decrease in the sea-ice coverage in the Labrador Sea (Fig. 11). BCM, HadCM3, IPSL-CM4 and IPSL-CM5 also show weak subtropical warming in the southeastern edge of the subtropical gyre, sometimes extending to the Caribbean Basin.

The SST anomalies lagging MOCy by only 2 year are shown in Fig. 10 (left panels). The positive SST anomalies were located closer to the Gulf Stream and the North Atlantic Current, indicating that they moved northward into the subpolar gyre, and in some cases also southward into the subtropical gyre.

East of Greenland, however, there are disagreements among models, especially in the Nordic Seas. Following a AMOC maximum, the Nordic Seas are indeed warm and

sea-ice retreats in BCM and HadCM3, while in IPSL-CM5 and KCM, and to a lesser extent IPSL-CM4 and MPI-ESM, the Nordic Seas are cold and sea ice expands. Since the atmospheric response to the AMOC is broadly similar in the six models, this suggests that the changes in the Nordic Seas induced by the AMOC have little impact on the large-scale atmospheric circulation. The subpolar region and Labrador Sea seem to exert the strongest effect onto the atmosphere. The polarity of the atmospheric response is consistent with the atmospheric response studies of Deser et al. (2004); Msadek et al. (2011), who found that positive SST anomalies in the subpolar North Atlantic can cause a negative phase of the NAO. Furthermore, a retreat of the Labrador sea ice cover was shown to produce a positive NAO response (Kvamstø et al. 2004; Alexander et al. 2004; Strong et al. 2009) which would oppose the atmospheric response in Fig. 7. The SST anomalies in the North Atlantic Current and the subpolar domain thus seem to be the main driver for the atmospheric response to the AMOC.

To highlight the links between the AMOC and the SST anomalies, we calculate an Atlantic Multidecadal Oscillation (AMO) index, defined as the yearly mean SST anomalies in the North Atlantic region (0°N – 60°N , 75°W – 7.5°E), after low-pass filtering with a Butterworth filter,

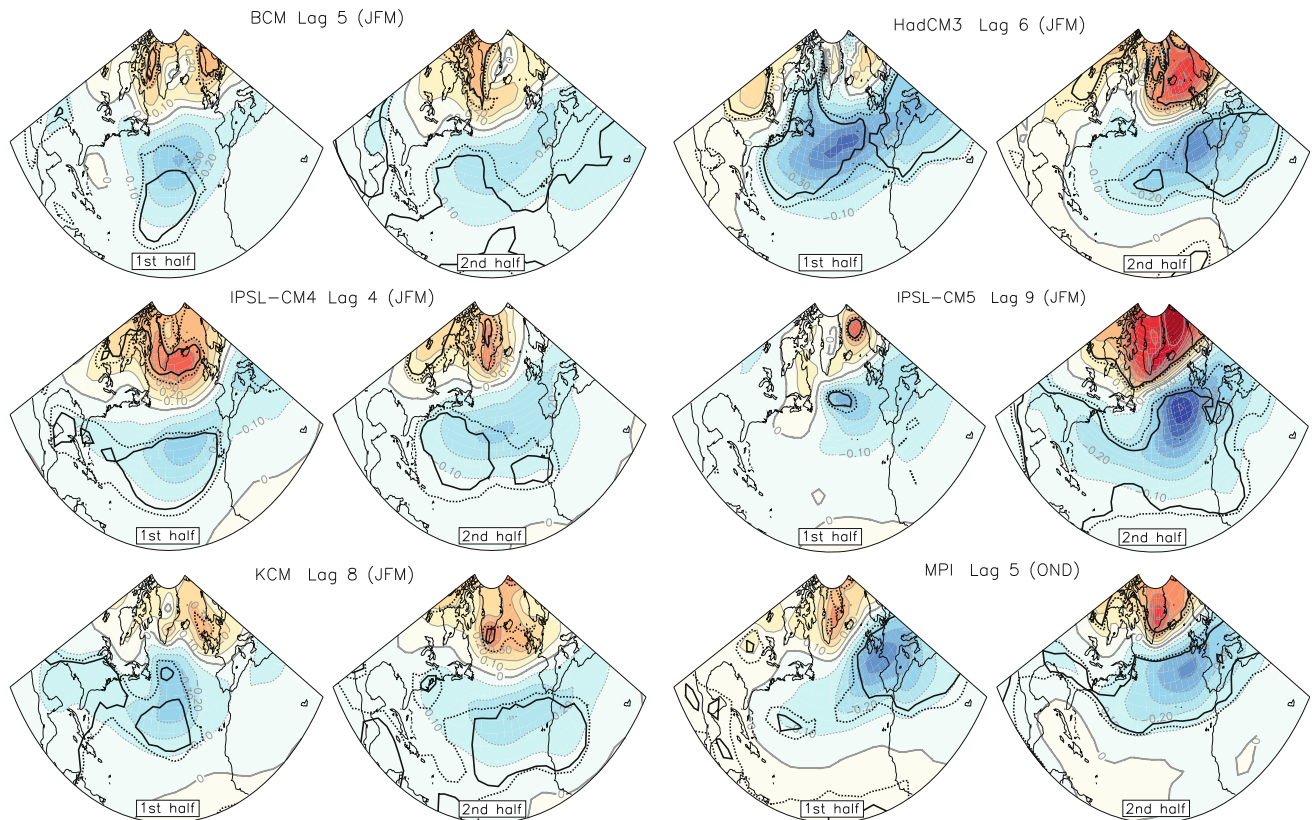


Fig. 8 Regression of the cold-season SLP onto MOCy, in hPa (colors), for the first and second half of the time series. The 5 and 10% significance levels are indicated with *continuous* and *dotted thick* contours, respectively

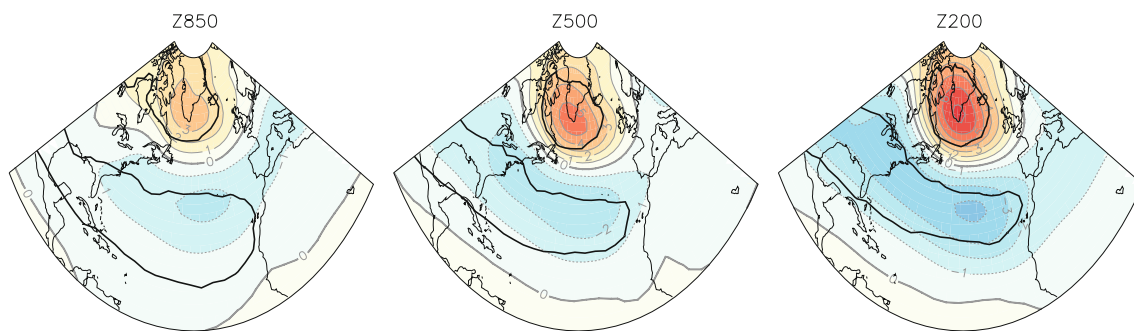


Fig. 9 Regression of the 850-, 500- and 200-hPa geopotential height onto MOCy, in m, for the JFM season in IPSL-CM4. The AMOC leads the atmosphere by 4 year. The *thick black contours* indicate the 5% significance

using a 10 year cutoff period. The SST patterns associated with the AMO are given in Fig. 12 by the regression of the SST anomalies onto the AMO index. In all models, there is a good correspondence between the structure of the AMO pattern and the SST anomalies induced by the AMOC (compare with Fig. 10), confirming that the AMOC is the cause of the low frequency variability of the North Atlantic SST. However, the SST anomalies associated with the AMO are much smoother and mostly positive in the whole domain. This likely reflects the smoothing effect of the

low-pass filtering and, possibly, the impact of tropical teleconnections (Guan and Nigam 2009; Compo and Sardeshmukh 2010).

4.2 Heat flux response

The links between the AMOC and the surface heat flux are difficult to assess. The variations of the AMOC change the oceanic heat advection, SST and sea-ice coverage, which induces heat flux anomalies denoted Q_O . If the atmosphere

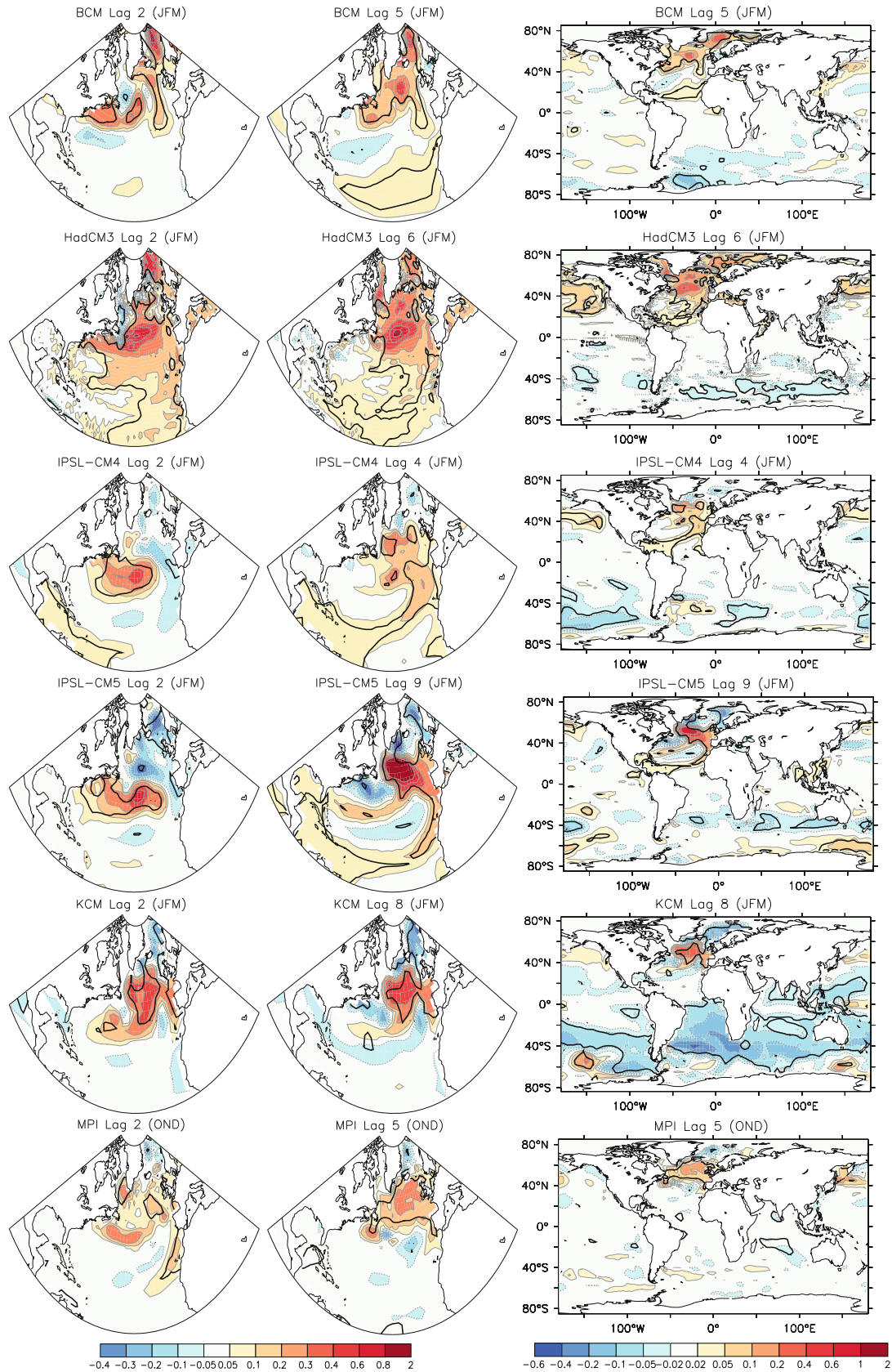


Fig. 10 Regression of the cold-season SST (K) onto MOCy, when MOCy leads SST by 2-year (*left panels*), and when the atmospheric response to the AMOC is most significant (*center and right panels*). The 5% significance is indicated by *thick black contours*

responds to the change in the boundary conditions, there is an additional heat flux anomaly that is the surface imprint of the large-scale atmospheric response, which is referred to as Q_A . The total heat flux anomaly associated with the AMOC, Q_{MOC} , may thus be separated into an oceanic and atmospheric component:

$$Q_{MOC} = Q_O + Q_A \quad (3)$$

The surface heat flux is the sum of the latent, sensible, shortwave and longwave heat fluxes, defined positive upward. We use as atmospheric index the time series associated to the SLP left singular vector in the first MCA mode, $a_1(t)$. It is highly correlated with the first PC of the SLP, which represents the NAO, consistent with the similarity in spatial patterns. The fraction of $a_1(t)$ reflecting the AMOC influence is obtained by multiplying $a_1(t)$ by R , the correlation between AMOC and SLP time series (see Fig. 7). Hence, Q_A is obtained by multiplying by R the heat flux regressed onto $a_1(t)$. Since Q_{MOC} is given by the regression of the heat flux onto MOCy, the response of the heat flux to the oceanic changes is obtained as a residual by $Q_O = Q_{MOC} - Q_A$.

Figure 13 illustrates the two components of the heat flux linked to the AMOC, Q_O and Q_A , for the lag of the strongest atmospheric response, except for HadCM3, where the heat fluxes were not available. For consistency, the ENSO signal was removed to the heat flux prior to analysis. The significance was estimated with Monte Carlo analysis, and heat flux anomalies larger than 3 W m^{-2} (respectively 1 W m^{-2}) are found to be significant at the 90% level for Q_O (Q_A). For reference, the mean heat flux during the cold-season is given by the contours in the left panels of Fig. 13, showing that the largest heat release to the atmosphere is located in the Gulf Stream/North Atlantic Current. Much heat is also lost in the subpolar gyre and the Nordic Seas.

After an intensification of the AMOC, the anomalous upward heat flux due to the oceanic changes, Q_O (left panels), has two maxima, one in the Gulf Stream/North Atlantic Current, and one in the subpolar gyre. These upward heat fluxes are associated with the large positive SST anomalies in Fig. 10 and reflect a negative heat flux feedback, as it acts to diminish the SST anomalies. Its magnitude compares well with that found in the observations (Frankignoul and Kestenare 2002; Park et al. 2005). In most models, there are also weaker patches of downward fluxes in the eastern North Atlantic. The atmospheric changes described by Q_A (right panels) are broadly consistent with the heat flux associated with a negative NAO phase, and they act to increase the heat loss in the subtropical gyre, while decreasing it in the subpolar gyre.

The atmospheric and oceanic components of the heat flux are comparable and add up in the Gulf Stream/North

Atlantic Current region. In the subpolar gyre, the negative heat flux feedback due to the strong SST anomalies dominates, hence the net heat flux anomaly is also upward in this region. It is suggested in the next section that these upward heat fluxes alter the lower-tropospheric flow and eventually generate a negative NAO pattern.

4.3 Storm track and eddy response

As we have a preferable access to this model, IPSL-CM4 is mainly used to discuss the atmospheric response to the AMOC. Even if the delayed atmospheric forcing of the AMOC is different in this model (see Fig. 6), it is well within the range of the other models in term of the delayed atmospheric response to the AMOC (see Fig. 7) and the analysis below likely applies to the other models.

To understand the atmospheric response to the AMOC, one needs to consider the changes of the atmospheric eddy field, which can be represented by the storm track activity, $(z_{500}^2)^{1/2}$, given here by the standard deviation of the bandpass (2.2-6 days) filtered 500 hPa geopotential, calculated from daily outputs (Blackmon 1976). As shown in the upper-left panel of Fig. 14, the strongest synoptic perturbations are located in a band from the coast of Newfoundland to the northern tip of the British Island, with a characteristic northeastward tilt (red contours). The storm track activity, $(z_{500}^2)^{1/2}$, is then regressed onto MOCy to estimate the perturbation associated with the AMOC (colors). A significant decrease of the eddy activity is found east of Newfoundland, while a gentle increase is found near the Caribbean Basin and over the northern Labrador Sea.

The Eady growth rate maximum, σ_{BI} , defined as $0.31 f |\partial u / \partial z| N^{-1}$, measures the intensity of the lower-tropospheric baroclinicity that governs the amplitude of the atmospheric perturbations (Hoskins and Valdes 1990) and the Rossby wave breaking (Rivière and Orlanski 2007). As shown in upper-right panel of Fig. 14, the major feature of the mean lower-tropospheric Eady growth rate maximum at 850-hPa (thick red contours) is the maximum located over the Gulf Stream region, from Cape Hatteras to the Grand banks of Newfoundland, upstream of the North Atlantic storm track. At 850 hPa, σ_{BI} decreases in response to the AMOC in the northern part of the strong-baroclinicity domain and it increases over the southwestern subtropical gyre and Florida. This corresponds to a southward shift and a weakening of the lower-tropospheric baroclinicity, which is clearly associated with the downstream decrease of the eddy activity.

The associated 200-hPa zonal wind anomalies show an enhanced zonality, with a weakening of the wind from Newfoundland and to the British Island and a strengthening of the subtropical jet over southern United States

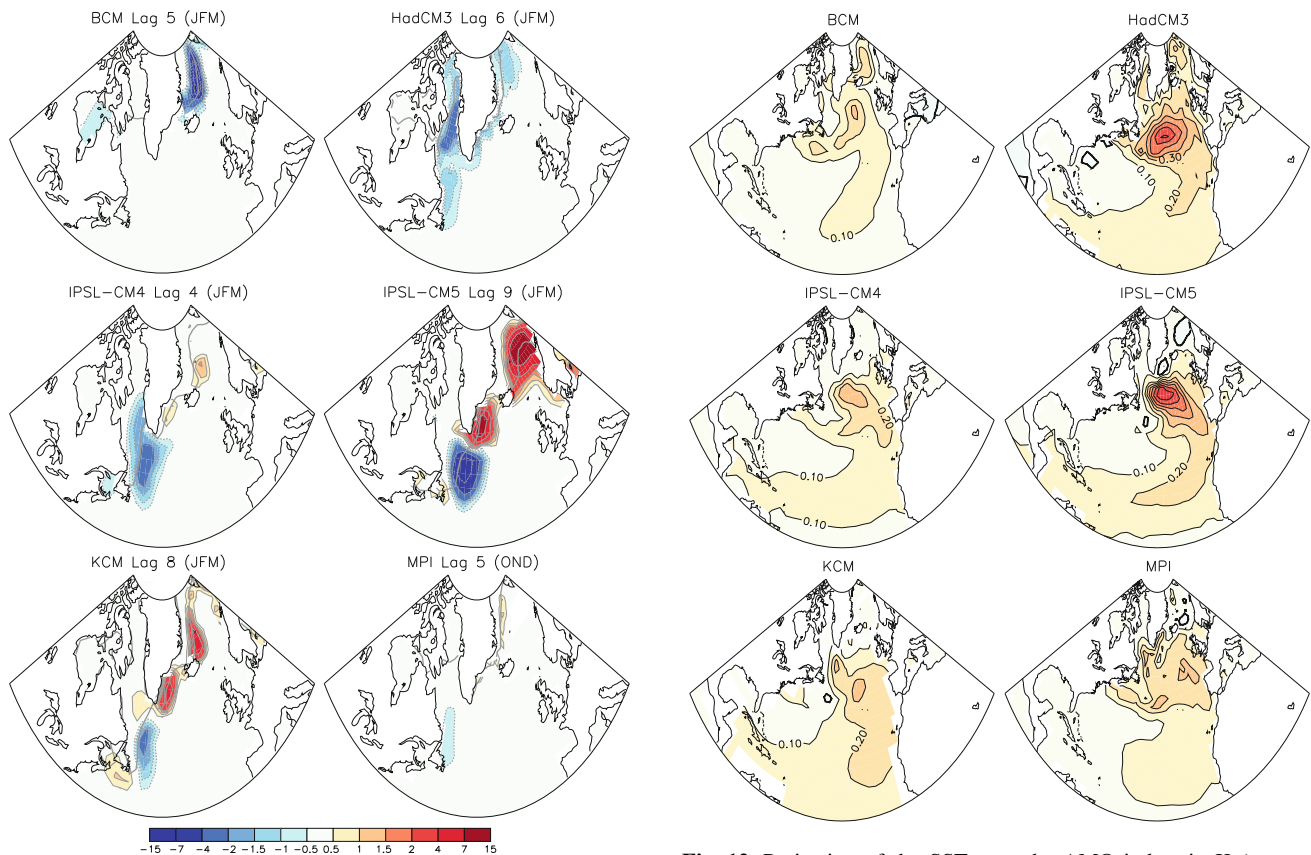


Fig. 11 Regression of the cold-season sea-ice cover (%) onto MOC_y , when the atmospheric response to the AMOC is most significant. The climatological sea-ice extent, corresponding to a sea-ice cover of 50%, is illustrated with a thick grey line. Note that all color contours are significant at the 10% level

and the Mediterranean region. (Fig. 14, lower left panel). The eddies usually transport momentum northward from the subtropical jet to the storm track region. As the baroclinicity weakens, the eddies transport less zonal momentum northward over the Atlantic Ocean, and the zonality of the flow is reinforced. These anomalies are consistent with the forcing tendency due to synoptic eddies in the development of a negative NAO (Doblas-Reyes et al. 2001).

Finally, we investigate the interactions between the eddy momentum fluxes and the mean flow with the E-vector, defined as $(1/2(\overline{v'^2} - \overline{u'^2}), -\overline{u'v'})$, where primes designate bandpass filtered quantities. Divergence (convergence) of the E-vector indicates zonal wind acceleration (deceleration) due to interaction between the transient eddies and the mean flow (Trenberth 1986). Some divergence is found in the subtropics (see lower-right Fig. 14), which amplifies the subtropical jet around 30°N, while the E-vectors converge over the storm track region west of the British Island and off Newfoundland. Therefore, the eddies act as a positive feedback and enhance the negative NAO pattern.

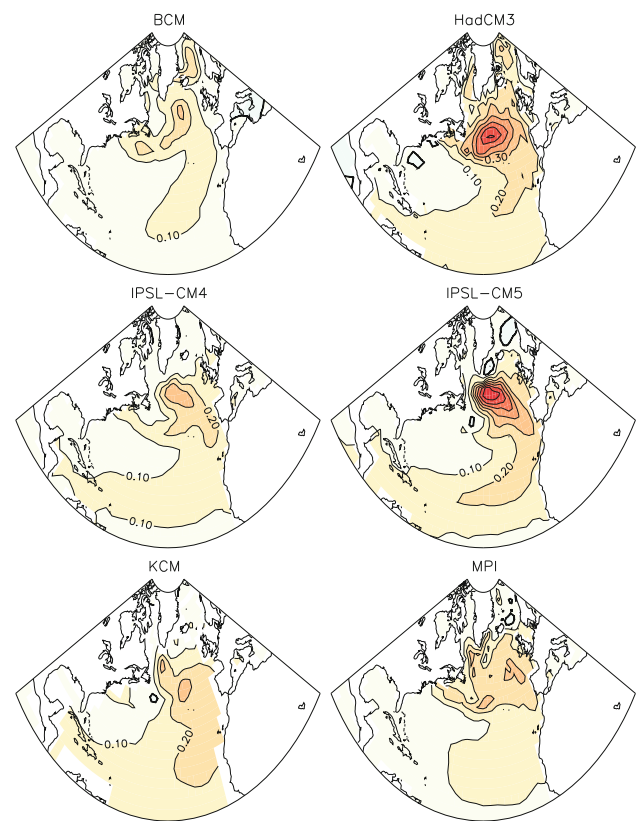


Fig. 12 Projection of the SST onto the AMO index, in K (contour interval 0.1 K). The AMO is defined as the yearly low-pass filtered SST anomalies, with a 10-year cutoff, averaged over the North Atlantic region (0°N–60°N, 75°W–7.5°E)

The mechanisms at work in IPSL-CM4 appear to be relevant to the other models. Indeed, there is a significant southward shift of the maximum Eady growth rate at the 850-hPa level in a broad region off Newfoundland in all the AOGCMs (Fig. 15), which confirms that eddy changes are associated with the atmospheric response to the AMOC. Over the Nordic Seas, there are discrepancies among models in the Eady growth rate maximum changes, consistent with the different SST and sea ice responses seen in Figs. 10 and 11.

In all models the atmospheric response to the AMOC strongly resembles the NAO in term of mechanism and spatial pattern. Therefore, it is difficult to distinguish the specificity of the AMOC response from the internal NAO dynamics. However, the lag established in the MCA suggests that the AMOC is primarily the cause of the atmospheric changes, while the corresponding SSTs suggest a strong influence of the warming in the subpolar North Atlantic region.

4.4 Climate impacts of the AMOC

Since the AMOC variability alters SST and sea ice cover in the North Atlantic and affects the atmospheric circulation,

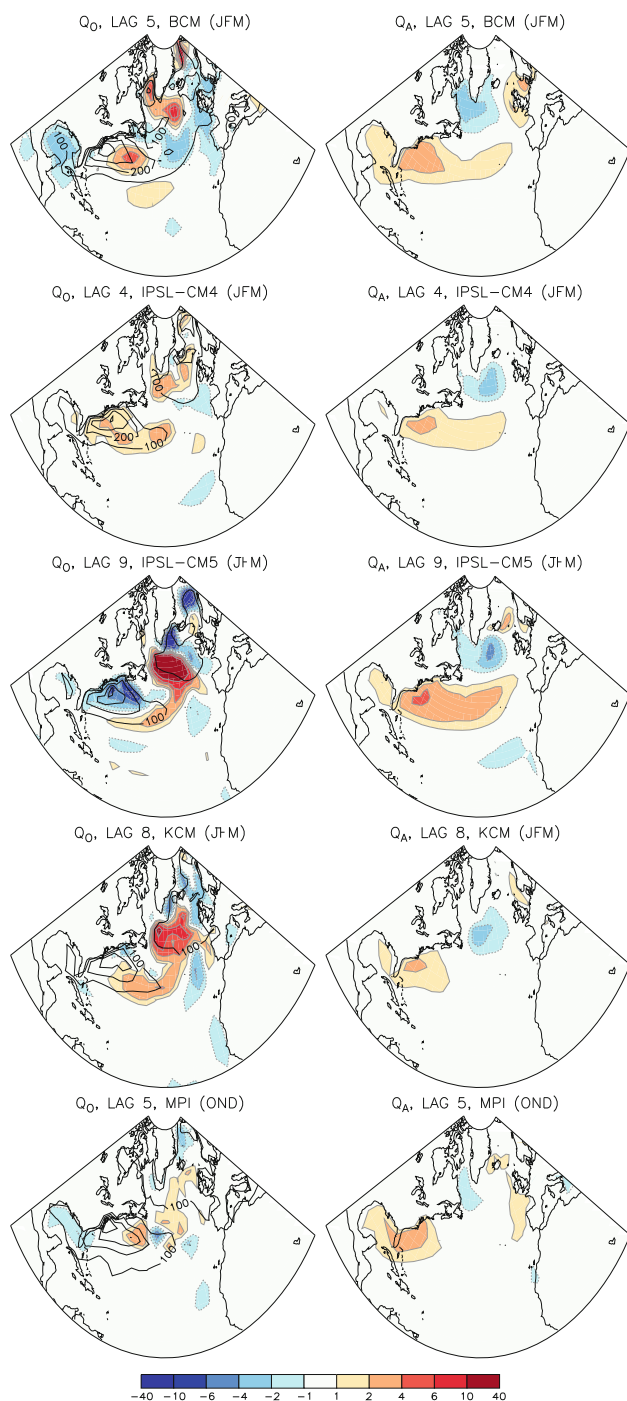


Fig. 13 Cold-season heat flux, in W m^{-2} , induced by the oceanic and atmospheric changes related to the AMOC, Q_O (left panels) and Q_A (right panels), in colors. The climatological mean of the heat flux Q , in W m^{-2} , is indicated in thin contours in the left panel. The color scale is non-linear

it may influence the climate of European and American regions. However, the atmospheric response is somewhat different among the models since, for example, the SLP patterns have slightly different center of actions among

models, albeit of similar amplitude and sign (see Fig. 7). To emphasize the similarities between the six models, Fig. 16 shows the response of the 850-hPa temperature, precipitation and SLP, averaged over all models, using the season and lag with the most significant atmospheric signature. The 850 hPa atmospheric temperature is used instead of the surface air temperature to focus on the large scale influence of the AMOC on climate processes, but the pattern and amplitude are similar. Again, ENSO was removed from all variables. Note that the thick contours in Fig. 16 indicate where the mean change is 5% significant, which mostly occurs when at least five of the models out of six give a signal of the same polarity.

The SLP changes reflect a negative phase (or cool phase) of the more global Arctic Oscillation (AO), as negative pressure anomalies are also observed over the North Pacific, while a high pressure anomaly is found over the North Pole. The 850 hPa temperature anomalies are broadly similar to the anomalies observed during a negative phase of the NAO/AO (Hurrell et al. 2003). Cold temperatures are found over much of the United States and southern Canada, while a band of warm temperature anomalies extends from the Labrador Sea to Western Europe, due to enhanced northerly and southerly flow over these regions, respectively. The temperature also increases over the Bering Strait and decreases in the band from the Philippine Archipelago to the Hawaiian Islands, which is consistent with the temperature advection linked with the SLP anomalies in the North Pacific, as found by Wu et al. (2008). A weak warming is also present over North Africa. Figure 17 gives the typical 850 hPa temperature changes in the North Atlantic sector for each model, to illustrate the model dependence of the cold-season impacts of the AMOC. The warming around Greenland and the Labrador Sea is mainly seen in HadCM3, IPSL-CM5 or MPI-ESM. The smaller warming over North Africa is especially strong for HadCM3. The cooling over North America is simulated in KCM, IPSL-CM4 or HadCM3, where it reaches -0.15 K, while the warming over the Western Europe is most significant in IPSL-CM5, where it reaches 0.1 K.

The rainfall strongly increases by about 0.05 mm day^{-1} over the subtropical Atlantic, from Southeastern United States to Spain and the Mediterranean Basin, while rainfall slightly, but significantly, decreases over Scandinavia and Scotland. This is due to the southward shift of the North Atlantic storm track that characterizes the negative phase of the NAO/AO. The subtropical Atlantic rainfall increase is much stronger than the decrease over the subpolar regions around the Nordic Seas, as the climatological mean rainfall is weaker over the subpolar regions. Precipitation is similarly enhanced over the subtropical eastern North Pacific Ocean, due to the negative AO and its associated southward shift of the

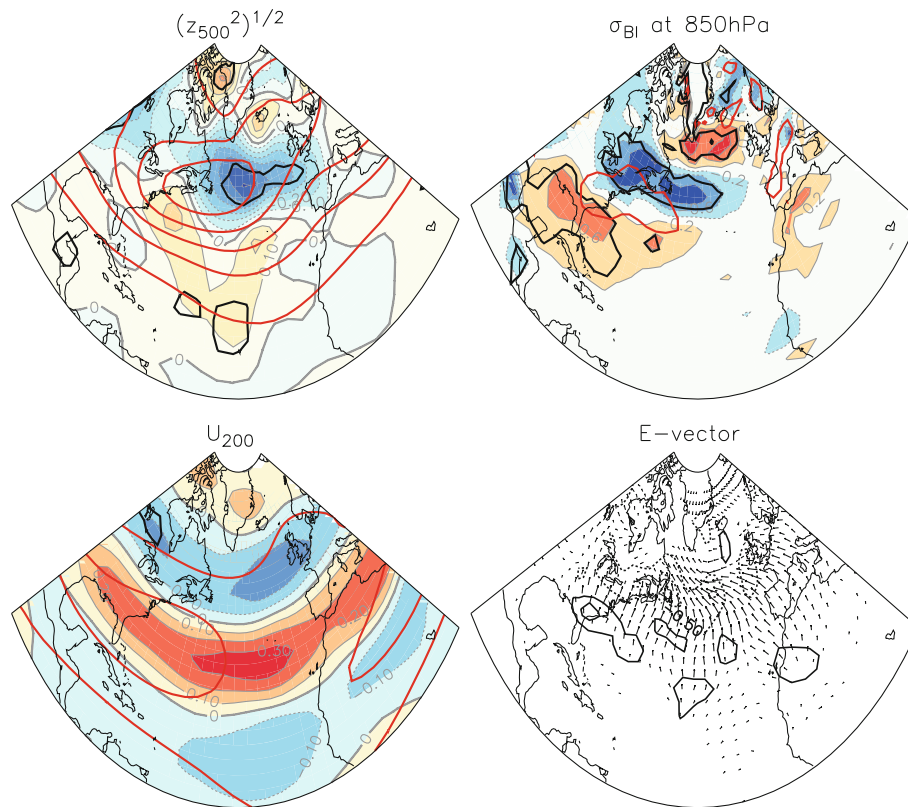


Fig. 14 Atmospheric eddy response to the AMOC, for the JFM season, in IPSL-CM4. (*Upper-left*) mean storm track activity, $\overline{z_{500}^2}^{1/2}$ in red contours, and lagged regression onto MOCy in colors. (*Upper-right*) mean Eady growth rate maximum at 850 hPa, σ_{BI} in red contours, and lagged regression onto MOCy (colors). (*Lower-left*) mean zonal wind at 200-hPa, U_{200} (red contours), and lagged regression onto MOCy (colors). (*Lower right*) Lagged regression of the E-vector $(1/2(\overline{v'^2} - \overline{u'^2}), \overline{u'v'})$ (vectors) and its divergence

(contours) at 200 hPa onto MOCy. MOCy leads atmosphere by 4 year in the lagged regressions. The thick black contours in all panels indicate the 5% significance level, except for lower panels. Contour intervals are 10 m for $\overline{z_{500}^2}$, 0.7 day^{-1} for σ_{BI} , 20 m s^{-1} for U_{200} , and $5 \times 10^{-5} \text{ m s}^{-2}$ for the E-vector divergence. Units for color shades are (upper-left) m, (upper-right) 10^{-2} day^{-1} , (lower-left) m s^{-1}

North Pacific storm track. An increase of precipitation is simulated over Gulf of Guinea and Equatorial Africa, which corresponds to the northward shift of the ITCZ (Intertropical Convergence Zone), usually associated with warm North Atlantic conditions (Sutton and Hodson 2005, 2007; Hodson et al. 2010). A significant decrease of precipitation is also found over the south-west Indian Ocean, which is associated in KCM with some negative SST anomalies (see Fig. 10) that could contribute to the NAO (Hurrell et al. 2004; Hoerling et al. 2004). However, the SST anomalies in the south-west Indian Ocean are very weak and not significant in the other models, and an important effect of this region for the midlatitudes seems unlikely. Hence, the precipitation decrease in the Indian ocean may reflect some remote influence of the ITCZ shift over the Atlantic Ocean and Equatorial Africa.

Finally, the strongest precipitation increase in Fig. 16 is found in the western equatorial Pacific. However, it mainly

reflects the large natural variability of precipitation in this region and it is not statistically significant. In fact, a strong and significant eastward shift of rainfall over the Indo-Pacific warm pool is only seen in one model, namely KCM (not shown). In this model, the centennial variability due to the Southern Ocean drives both the AMOC and the tropical precipitation in the Indo-Pacific region (Park and Latif 2008).

5 Discussion and conclusion

The atmospheric signature of the natural variability of the AMOC was studied in multi-centennial control simulations with six AOGCMs, using a lagged MCA between the yearly AMOC and seasonal averages of SLP over the North Atlantic sector. A significant equivalent barotropic atmospheric response was found in all models in the cold-season, with a time lag between 1 and 10 year, depending on

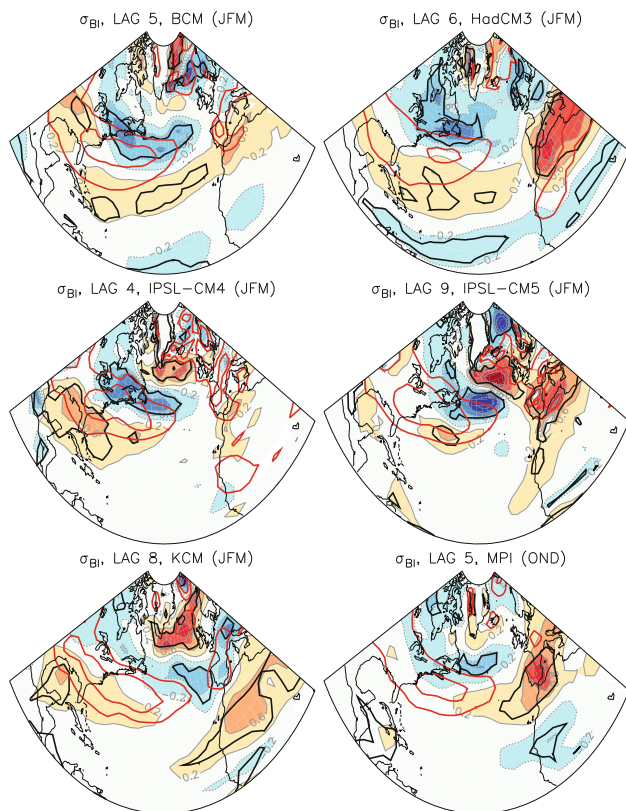


Fig. 15 Eady growth rate maximum at 850 hPa in response to the AMOC, for the cold-season. The climatological mean Eady growth rate maximum is indicated in *red contours*, with a contour interval of 0.7 day^{-1} , while the regression of the Eady growth rate maximum onto MOCy is shown with *colors*, in 10^{-2} day^{-1} . The *thick black contours* indicate the 5% significance level

the AOGCM. In all cases, an AMOC intensification leads to SLP anomalies that resemble a negative phase of the NAO, and conversely an AMOC weakening leads to a positive NAO. For a typical yearly fluctuation of the AMOC, the SLP signal ranges between 0.4 and 0.8 hPa, which matches 10–15% of the anomalies of the seasonal NAO. The atmospheric response affects the climate over the whole North Atlantic region. In the multi-model average, there is a significant increase of the rainfall of about 0.05 mm day^{-1} over the northern subtropical Atlantic Ocean and a weaker increase of about 0.02 mm day^{-1} over Spain, the Mediterranean region and southern North America. In addition, there is a cooling of 0.1 K over most of the North American continent, and a warming of 0.15 K over a broad band extending from the Labrador Sea to Western Europe. We also note some weaker warming over Sahara and northern North Pacific. These climate impacts of the AMOC are present in each model, even if there are large differences in amplitude or spatial pattern, with HadCM3 and IPSL-CM5 having the largest AMOC impacts and MPI-ESM the smallest. The climatic impacts of the AMOC appear to be weak at first sight. However, as

the frequency spectrum of the AMOC is red and that of atmosphere essentially white, the AMOC influence should become more visible at low frequency. For instance, using a lowpass filter with a 20-year cutoff typically triples the ratio between AMOC and SLP fluctuations. Therefore, in the models, the percentage of NAO amplitude explained by the AMOC could exceed 30% on multidecadal timescales, based on the present findings. Hence, the AMOC may be an important driver of low frequency variability of the NAO, even though it may be hard to establish using low-pass data since the cause and effect of the AMOC fluctuations may not be distinguishable.

The physical mechanisms leading to the atmospheric response were investigated. The AMOC intensification increases the northward oceanic heat transport, which primarily results in warm SST anomalies that propagate along the North Atlantic Current to the subpolar gyre and the Labrador Sea. The positive SST anomalies are damped by the negative heat flux feedback, resulting in an anomalous heat release over the Gulf Stream/North Atlantic Current and much of the subpolar gyre. In most models, this upward heat flux should warm the lowest tropospheric layers and modify the baroclinicity in the subpolar region. Indeed, a southward shift of the baroclinicity is found upstream of the North Atlantic storm track, off the coast of Newfoundland, while the storm track activity weakens. The atmospheric eddies transport less heat and vorticity poleward, which further acts to amplify the negative phase of the NAO/AO. As SST anomalies in the Nordic Seas are not consistent between models, at the lag where the atmospheric response is detected in the MCA, this region does not seem to play an important role in the response. Similarly, the retreat of sea ice in the Labrador Sea is unlikely to be the cause of the atmospheric circulation changes as simulations and observations suggest that it should result in a positive NAO response (e.g., Kvamstø et al. 2004; Alexander et al. 2004; Strong et al. 2009).

Finally, although the ENSO signal was rather crudely subtracted and could have been filtered in a more efficient way (Penland and Matrosova 2006), albeit more onerously, and the possible influence of Indian ocean anomalies was not filtered out, it seems very unlikely that tropical SST anomalies play a significant role in the detected atmospheric response. Indeed, in all models but KCM the tropical SST anomalies associated with the AMOC were very small and not significant after ENSO filtering. In KCM, both the AMOC and the tropical variability are linked to some strong centennial variability originated in the Southern Ocean (Park and Latif 2008). Hence, the AMOC influence seems to be primarily due to the SST anomalies in the North Atlantic subpolar region. The atmospheric changes are consistent with the mechanisms established in previous studies (Peng et al. 2003; Ferreira

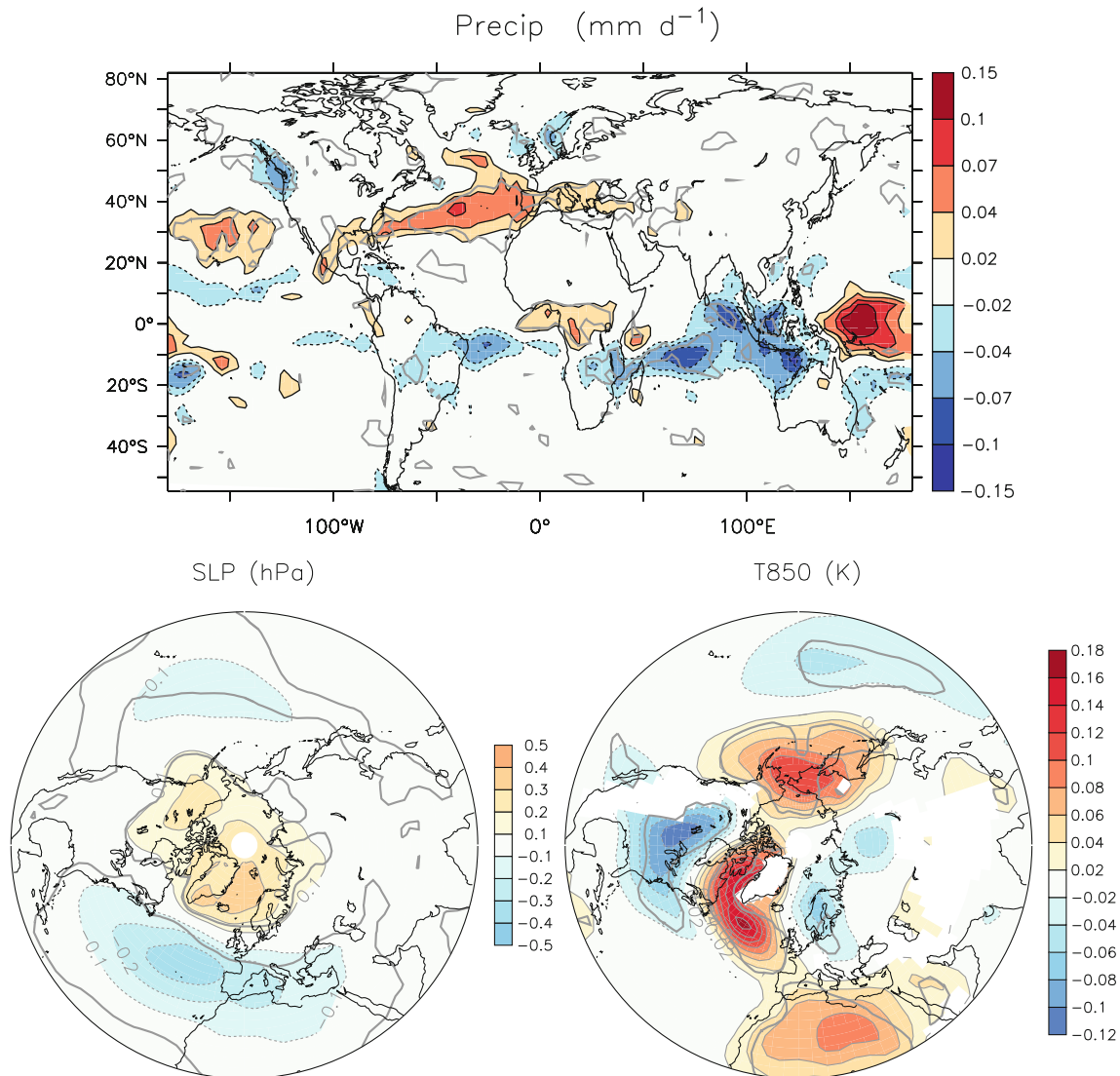


Fig. 16 Regressions of the cold-season precipitation (mm day^{-1}), SLP (hPa) and 850-hPa temperature (K) onto MOCy, averaged for IPSL-CM4, BCM, KCM, MPI-ESM, HadCM3 and IPSL-CM5, during the strongest atmospheric response to the AMOC. The *thick gray lines* indicate the regions where the changes are different from

zero, at the 5% significance, as given by a student *t*-test. The zero contour is omitted for clarity. The color scale used for precipitation is non-linear. In *lower left panel*, the regions where the surface pressure can be below 850 hPa are also omitted

and Frankignoul 2005; Deser et al. 2007). However, it should be remarked that the changes in the transient eddy statistics that we attributed to the AMOC forcing are also broadly characteristic of a negative NAO phase, so that they do not per se demonstrate causality, even if they show consistency. What strongly suggests causality is the lag between the AMOC intensification, the warming of the subpolar domain, and the atmospheric signal. Additional experiments using atmospheric models are needed to further assess the role of the SST and heat flux anomalies.

As the NAO is a main forcing of the AMOC variability in many oceanic hindcats (e.g., Eden and Willebrand 2001; Deshayes and Frankignoul 2008), the atmospheric response

to the AMOC should act as a feedback and thus play an active role in setting the variability of the AMOC. This appear to be the case in two coupled models, namely BCM and HadCM3, where a positive NAO leads to a strengthening of the AMOC, which is seen in the MCA with up to 7 year lag. As the strengthening of the AMOC generates a negative NAO phase about 5 years later, the atmospheric response should act as a delayed negative feedback, perhaps leading to a reversal of the sign of the AMOC anomaly. This should enhance the decadal variability in the two models, consistent with the mechanism discussed in Farneti and Vallis (2009). However, as the atmospheric response to the AMOC is weak, it remains to be established

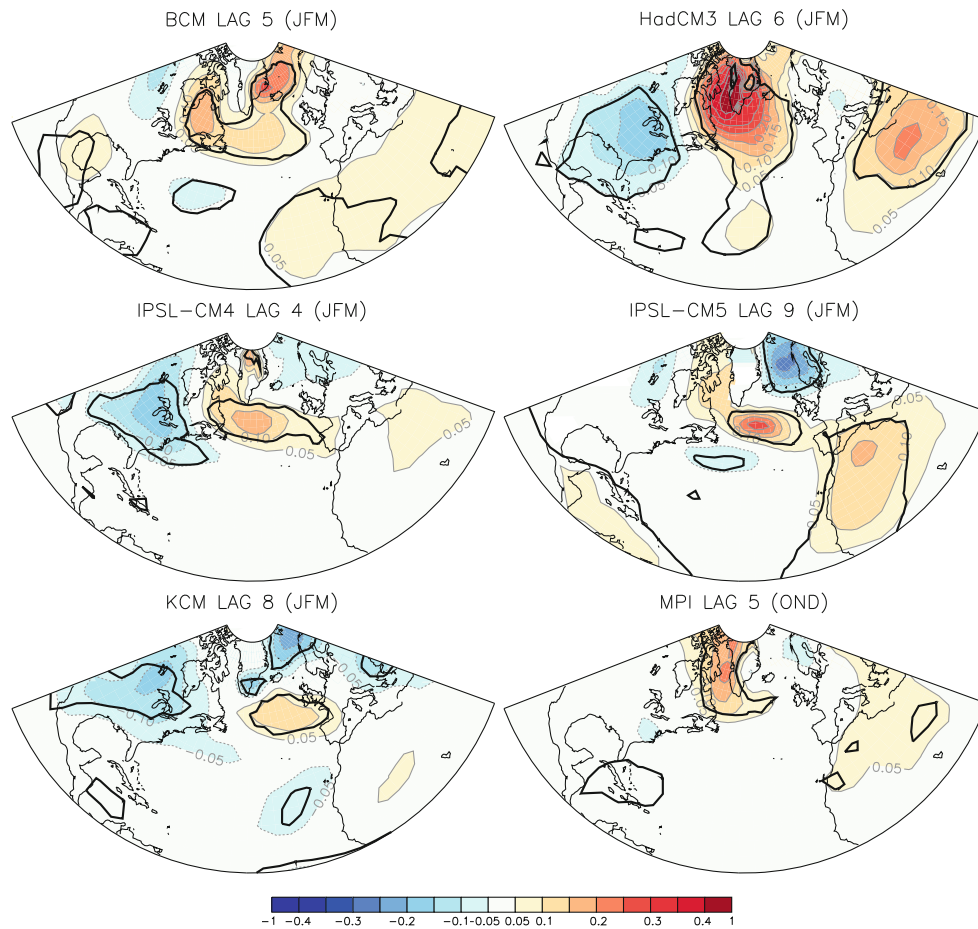


Fig. 17 Regressions of the cold-season 850-hPa temperature (K) onto MOCy, for individual models during the strongest atmospheric response to the AMOC. The *thick black contours* indicate the 5% significance level. The zero contour is omitted for clarity

if this active air-sea coupling has a significant influence on the AMOC time scales, which may be largely controlled by internal ocean variability (Delworth et al. 1993; Dong and Sutton 2005). Conversely, in the other four models, the NAO does not seem to play a leading role in driving the AMOC variability. Hence, no particular feedback is expected from the atmospheric response.

Interestingly, in the models the rainfall caused by the AMOC differs from that seen in simulations forced by the SST anomalies derived from the observed AMO. As shown by Sutton and Hodson (2005, 2007) and Hodson et al. (2010), a warm phase of the AMO indeed causes widespread negative SLP anomalies centered around 40°N in the Atlantic Ocean, especially during the warm season. Kushnir et al. (2010) report for the cold season some similarities with the AMOC impact on precipitation described here. However, this response appears to be primarily driven by the large tropical Atlantic SST anomalies, that drive an off-equatorial Gill response over the Caribbean Basin and a shift of the Atlantic ITCZ. In the present study, the AMOC-induced SST anomalies are small in the

tropics, and the extratropical SST anomalies thus play the dominant role.

Our results are encouraging for the decadal predictability of climate, since the AMOC may be predictable up to a decade ahead (Collins et al. 2006). Hence, some of the NAO variability might also be predictable. Climate coupled model simulations under the scenario A1B of moderate greenhouse gases emission suggest that the AMOC should decrease by 25% at the end of the 21st century (Schmittner et al. 2005). This corresponds to a decrease of about 4 Sv. A composite analysis of the atmospheric conditions following a strong and weak AMOC shows that the atmospheric response found in this study is approximately linear (not shown). The expected weakening of the AMOC could lead in global warming conditions to climate anomalies four time stronger, corresponding for example to a cooling of up to 0.5 K over part of North America, based on the multi-model average. The AMOC weakening could thus modulate significantly the global warming amplitude at regional scale.

A word of caution is required. Even though the models considered in this study show a consistent influence of the

AMOC onto the atmospheric circulation during the cold season, they have limitations and other climate models may behave differently, in particular as the model resolution increases. As will be reported elsewhere, work in progress shows that CCSM3 indeed behaves differently, even though the mechanisms suggested here remain relevant. In higher resolution simulations, the atmospheric response induced by sharp SST fronts is likely to play a somewhat more important role (Nakamura et al. 2004; Minobe et al. 2008). This stresses the importance of investigating further the processes that control the atmospheric response to boundary forcing.

Acknowledgments The research leading to these results has received funding from the European Community's 7th framework programme (FP7/2007–2013) under grant agreement No. GA212643 (THOR: “Thermohaline Overturning—at Risk”, 2008–2012). For CF, support from the Institut Universitaire de France is gratefully acknowledged. We also thank T. Joyce, J. Mignot, and two anonymous reviewers for their useful comments and suggestions.

References

- Alexander MA, Bhatt US, Walsh JE, Timlin MS, Miller JS, Scott JD (2004) The atmospheric response to realistic Arctic sea ice anomalies in an AGCM during winter. *J Clim* 17(5):890–905
- Balmaseda M, Ferranti L, Molteni F, Palmer T (2010) Impact of 2007 and 2008 Arctic ice anomalies on the atmospheric circulation: implications for long-range predictions. *Q J R Meteorol Soc* 136:1655–1664. doi:10.1002/qj.661
- Bentsen M, Drange H, Furevik T, Zhou T (2004) Simulated variability of the Atlantic meridional overturning circulation. *Clim Dyn* 22(6):701–720
- Blackmon ML (1976) A climatological spectral study of the 500-mb geopotential height of the northern hemisphere wintertime circulation. *J Atmos Sci* 33:1607–1623
- Bretherton CS, Smith C, Wallace JM (1992) An intercomparison of methods for finding coupled patterns in climate data. *J Clim* 5(6):541–560
- Cassou C, Deser C, Alexander MA (2007) Investigating the impact of reemerging sea surface temperature anomalies on the winter atmospheric circulation over the North Atlantic. *J Clim* 20(14):3510–3526
- Collins M et al (2006) Interannual to decadal climate predictability in the North Atlantic: a multimodel-ensemble study. *J Clim* 19(7):1195–1203
- Compo GP, Sardeshmukh PD (2010) Removing ENSO-related variations from the climate record. *J Clim* 23(8):1957–1978
- Cunningham SA et al (2007) Temporal variability of the Atlantic meridional overturning circulation at 26.5N. *Science* 317(5840):935–938. doi:10.1126/science.1141304
- Czaja A, Frankignoul C (1999) Influence of the North Atlantic SST on the atmospheric circulation. *Geophys Res Lett* 26:2969–2972
- Czaja A, Frankignoul C (2002) Observed impact of Atlantic SST anomalies on the North Atlantic oscillation. *J Clim* 15(6):606–623
- Danabasoglu G (2008) On multidecadal variability of the Atlantic meridional overturning circulation in the community climate system model version 3. *J Clim* 21(21):5524–5544
- Delworth T, Manabe S, Stouffer RJ (1993) Interdecadal variations of the thermohaline circulation in a coupled ocean-atmosphere model. *J Clim* 6(11):1993–2011
- Delworth TL, Greatbatch RJ (2000) Multidecadal thermohaline circulation variability driven by atmospheric surface flux forcing. *J Clim* 13(9):1481–1495
- Deser C, Magnusdottir G, Saravanan R, Phillips A (2004) The effects of North Atlantic SST and sea ice anomalies on the winter circulation in CCM3. Part II: direct and indirect components of the response. *J Clim* 17(5):877–889
- Deser C, Tomas RA, Peng S (2007) The transient atmospheric circulation response to North Atlantic SST and sea ice anomalies. *J Clim* 20(18):4751–4767
- Deshayes J, Frankignoul C (2008) Simulated variability of the circulation in the North Atlantic from 1953 to 2003. *J Clim* 21(19):4919–4933
- Doblas-Reyes FJ, Pastor MA, Casado MJ, Déqué M (2001) Wintertime westward-traveling planetary-scale perturbations over the Euro-Atlantic region. *Clim Dyn* 17:811–824
- Dong B, Sutton RT (2005) Mechanism of interdecadal thermohaline circulation variability in a coupled Ocean-Atmosphere GCM. *J Clim* 18(8):1117–1135
- Dufresne J-L et al (2010) IPSL earth system model. Technical report, Institut Pierre Simon Laplace, Paris, France
- Eden C, Greatbatch RJ (2003) A damped decadal oscillation in the North Atlantic climate system. *J Clim* 16(24):4043–4060
- Eden C, Willebrand J (2001) Mechanism of interannual to decadal variability of the North Atlantic circulation. *J Clim* 14(10):2266–2280
- Farneti R, Vallis GK (2009) Mechanisms of interdecadal climate variability and the role of ocean-atmosphere coupling. *Clim Dyn*. doi:10.1007/s00382-009-0674-9
- Ferreira D, Frankignoul C (2005) The transient atmospheric response to midlatitude SST anomalies. *J Clim* 18(7):1049–1067
- Frankcombe LM, von der Heydt A, Dijkstra HA (2010) North Atlantic multidecadal climate variability: an investigation of dominant time scales and processes. *J Clim* 23(13):3626–3638
- Frankignoul C, Kestenare E (2002) The surface heat flux feedback. Part I: estimates from observations in the Atlantic and the North Pacific. *Clim Dyn* 19:633–647
- Frankignoul C, Kestenare E (2005) Air-sea interactions in the tropical Atlantic: a view based on lagged rotated maximum covariance analysis. *J Clim* 18(18):3874–3890
- Ganachaud C, Wunsch C (2000) Improved estimates of global ocean circulation, heat transport and mixing from hydrographic data. *Nature* 408:453–457
- Griffies SM, Tziperman E (1995) A linear thermohaline oscillator driven by stochastic atmospheric forcing. *J Clim* 8(10):2440–2453
- Guan B, Nigam S (2009) Analysis of Atlantic SST variability factoring interbasin links and the secular trend: clarified structure of the Atlantic Multidecadal Oscillation. *J Clim* 22(15):4228–4240
- Hodson D, Sutton R, Cassou C, Keenlyside N, Okumura Y, Zhou T (2010) Climate impacts of recent multidecadal changes in Atlantic Ocean sea surface temperature: a multimodel comparison. *Clim Dyn* 34:1041–1058
- Hoerling MP, Hurrell JW, Xu T, Bates GT, Phillips A (2004) Twentieth century North Atlantic climate change. Part II: understanding the effect of Indian Ocean warming. *Clim Dyn* 23:391–405
- Hoskins BJ, Valdes PJ (1990) On the existence of storm-tracks. *J Atmos Sci* 47(15):1854–1864
- Hurrell J, Kushnir Y, Visbeck M, Ottersen G (2003) An overview of the North Atlantic oscillation. In: Hurrell JW, Kushnir Y, Ottersen G, Visbeck M (eds) *The North Atlantic oscillation, climatic significance and environmental impact*, AGU Geophysical Monograph, vol 134, pp 1–35

- Hurrell JW, Hoerling MP, Phillips A, Xu T (2004) Twentieth century North Atlantic climate change. Part I: assessing determinism. *Clim Dyn* 23:371–389
- Jungclauss JH et al (2010) Climate and carbon-cycle variability over the last millennium. *Clim Past* 6(5):723–737
- Knight J, Allan R, Folland C, Vellinga M, Mann M (2005) A signature of persistent natural thermohaline circulation cycles in observed climate. *Geophys Res Lett* 32:L20708. doi:[10.1029/2005GL024233](https://doi.org/10.1029/2005GL024233)
- Kushnir Y, Seager R, Ting M, Naik N, Nakamura J (2010) Mechanisms of tropical Atlantic SST influence on North American precipitation variability. *J Clim* 23(21):5610–5628
- Kvamstø N, Skeie P, Stephenson D (2004) Impact of Labrador sea-ice extent on the North Atlantic oscillation. *Int J Climatol* 26:603–612
- Kwon Y-O, Alexander MA, Bond NA, Frankignoul C, Nakamura H, Qiu B, Thompson LA (2010) Role of the Gulf Stream and Kuroshio-Oyashio systems in large-scale atmosphere-ocean interaction: a review. *J Clim* 23(12):3249–3281
- Latif M et al (2004) Reconstructing, monitoring, and predicting multidecadal-scale changes in the North Atlantic thermohaline circulation with sea surface temperature. *J Clim* 17(7):1605–1614
- Lau N-C, Nath MJ (1990) A General Circulation Model study of the atmospheric response to extratropical SST anomalies observed in 1950–79. *J Clim* 3(9):965–989
- Magnusdottir G, Deser C, Saravanan R (2004) The effects of North Atlantic SST and sea ice anomalies on the winter circulation in CCM3. Part I: main features and storm track characteristics of the response. *J Clim* 17(5):857–876
- Marti O et al (2010) Key features of the IPSL ocean atmosphere model and its sensitivity to atmospheric resolution. *Clim Dyn* 34:1–26
- Mathieu P-P, Sutton RT, Dong B, Collins M (2004) Predictability of winter climate over the North Atlantic European region during ENSO events. *J Clim* 17(10):1953–1974
- McManus J, Francois R, Gherardi J-M, Keigwin L, Brown-Leger S (2004) Collapse and rapid resumption of Atlantic meridional circulation linked to deglacial climate changes. *Nature* 428:834–837
- Mikolajewicz U, Maier-Reimer E (1990) Internal secular variability in an ocean general circulation model. *Clim Dyn* 4(3):145–156
- Minobe S, Kuwano-Yoshida A, Komori N, Xie S-P, Small RJ (2008) Influence of the Gulf Stream on the troposphere. *Nature* 452:206–209
- Msadek R, Frankignoul C (2009) Atlantic multidecadal oceanic variability and its influence on the atmosphere in a climate model. *Clim Dyn* 33:45–62
- Msadek R, Frankignoul C, Li Z (2011) Mechanisms of the atmospheric response to the North Atlantic multidecadal variability: a model study. *Clim Dyn* 36(7):1255–1276
- Nakamura H, Sampe T, Tanimoto Y, Shimpo A (2004) Observed associations among storm tracks, jet streams and midlatitude oceanic fronts. *Earth Clim Ocean Atmos Interact Geophys Monogr* 147:329–346
- Otterå O, Bentsen M, Drange H, Suo L (2010) External forcing as a metronome for Atlantic multidecadal variability. *Nat Geosci* 3:688–694
- Park S, Deser C, Alexander MA (2005) Estimation of the surface heat flux response to sea surface temperature anomalies over the global oceans. *J Clim* 18(21):4582–4599
- Park W, Keenlyside N, Latif M, Ströh A, Redler R, Roeckner E, Madec G (2009) Tropical Pacific climate and its response to global warming in the Kiel Climate Model. *J Clim* 22(1):71–92
- Park W, Latif M (2008) Multidecadal and multicentennial variability of the meridional overturning circulation. *Geophys Res Lett* 35:L22703. doi:[10.1029/2008GL035779](https://doi.org/10.1029/2008GL035779)
- Peng S, Robinson WA, Li S (2003) Mechanisms for the NAO responses to the North Atlantic SST tripole. *J Clim* 16(12):1987–2004
- Peng S, Whitaker JS (1999) Mechanisms determining the atmospheric response to midlatitude SST anomalies. *J Clim* 12(5):1393–1408
- Penland C, Matrosova L (2006) Studies of El Niño and interdecadal variability in tropical sea surface temperatures using a nonnormal filter. *J Clim* 19(22):5796–5815
- Pohlmann H, Sienz F, Latif M (2006) Influence of the multidecadal Atlantic meridional overturning circulation variability on European climate. *J Clim* 19(23):6062–6067
- Rivière G, Orlandi I (2007) Characteristics of the Atlantic storm-track eddy activity and its relation with the North Atlantic Oscillation. *J Atmos Sci* 64(2):241–266
- Rodwell DP, Folland CK, Maskell K, Ward MN (1995) Variability of summer rainfall over tropical north Africa (1906–92): observations and modelling. *Q J R Meteorol Soc* 121:669–704
- Schmittner A, Latif M, Schneider B (2005) Model projections of the North Atlantic thermohaline circulation for the 21st century assessed by observations. *Geophys Res Lett* 32:L23710. doi:[10.1029/2005GL024368](https://doi.org/10.1029/2005GL024368)
- Schott FA, Fischer J, Dengler M, Zantopp R (2006) Variability of the deep western boundary current east of the grand banks. *Geophys Res Lett* 33:L21S07. doi:[10.1029/2006GL026563](https://doi.org/10.1029/2006GL026563)
- Stouffer RJ et al (2006) Investigating the causes of the response of the thermohaline circulation to past and future climate changes. *J Clim* 19(8):1365–1387
- Strong C, Magnusdottir G (2010) The role of Rossby wave breaking in shaping the equilibrium atmospheric circulation response to North Atlantic boundary forcing. *J Clim* 23(6):1269–1276
- Strong C, Magnusdottir G, Stern H (2009) Observed feedback between winter sea ice and the North Atlantic Oscillation. *J Clim* 22(22):6021–6032
- Sutton RT, Hodson DLR (2007) Climate response to basin-scale warming and cooling of the North Atlantic Ocean. *J Clim* 20(5):891–907
- Sutton RW, Hodson DLR (2005) Atlantic Ocean forcing of North American and European summer climate. *Science* 309:115–118
- Timmermann A, Latif M, Voss R, Grötzner A (1998) Northern hemispheric interdecadal variability: a coupled air-sea mode. *J Clim* 11(8):1906–1931
- Timmermann A et al (2007) The influence of a weakening of the Atlantic meridional overturning circulation on ENSO. *J Clim* 20(19):4899–4919
- Trenberth KE (1986) An assessment of the impact of transient eddies on the zonal flow during a blocking episode using localized Eliassen-Palm flux diagnostics. *J Atmos Sci* 43(19):2070–2087
- Trenberth KE, Caron JM (2001) Estimates of meridional atmosphere and ocean heat transports. *J Clim* 10:3433–3443
- Trenberth KE, Shea DJ (2006) Atlantic hurricanes and natural variability in 2005. *Geophys Res Lett* 33:L12704. doi:[10.1029/2006GL026894](https://doi.org/10.1029/2006GL026894)
- Vellinga M, Wu P (2004) Low-latitude freshwater influence on centennial variability of the Atlantic thermohaline circulation. *J Clim* 17(23):4498–4511
- Wu L, Li C, Yang C, Xie S-P (2008) Global teleconnections in response to a shutdown of the Atlantic meridional overturning circulation. *J Clim* 21(12):3002–3019
- Zhang R (2008) Coherent surface-subsurface fingerprint of the Atlantic Meridional Overturning Circulation. *Geophys Res Lett* 35:L20705. doi:[10.1029/2008GL035463](https://doi.org/10.1029/2008GL035463)